

1 **Response to Reviewers and modifications to manuscript**
2 **acp-2019-1001**

3

4 **Contents**

5	Response to RC1	2
6	Response to RC2	23
7	Tracked Changes Manuscript	28
8	Abstract	29
9	1. Introduction	30
10	2. Instrumentation	33
11	3. Davis 24 year rotational temperature dataset	34
12	4. Trend Assessment	40
13	5. Discussion	53
14	6. Summary and Conclusions	67
15	Data Availability	69
16	Author Contribution	69
17	Competing Interests	70
18	Acknowledgements	70
19	References	70

20

21

22 Response to RC1

23

24 Review of "Analysis of 24 years of mesopause region OH rotational temperature
25 observations at Davis, Antarctica. Part 1: Long-term trends" by French et al.

26

27 This manuscript presents the analysis of a very long dataset of OH temperatures over
28 Antarctica. This is an extension of 8 years of the dataset presented by French and
29 Klekociuk (2011). Indeed, results for the trends derived here coincide with their previous
30 results and those for the solar response are only slightly different. In this work, the
31 authors further identify and isolate a close-to-4-year period signal, which is to be
32 studied

33 in the second part of this work. Even if the results in this paper may initially look as a
34 mere update of previous results using an extended database, they are interesting and
35 certainly worth publishing because they show the persistence of the trend and the
36 consistency of the solar signal. Therefore, I suggest the publication of this paper in ACP,
37 once the following concerns and comments are taken into account.

38

39 Line numbering corresponds to the latest version uploaded by the authors (acp-2019-
40 1001-manuscript-version3.pdf).

41

42 [Thank you for your considered and detailed review of acp-2019-1001. We address your
43 comments and suggestions below.](#)

44

45 Main comments

46

47 There is no discussion on the effect of MLS broad vertical resolution in the mesosphere
48 and the potential impact on the comparisons shown in the manuscript. Indeed, it would be
49 interesting to see comparisons with SABER, even with a smaller winter temporal-
50 coverage. Additionally, SABER provides information on the altitude of the OH layer,
51 potentially providing a more accurate approach. In the same context, the choice of a fixed
52 pressure level in MLS data (seemingly done based just on a better agreement) is not very
53 well justified, as the layer altitude varies.

54

55 [The broad vertical resolution \(15km averaging kernel\) of MLS profiles in the mesopause
56 region is referenced on line 290. Its effect is to integrate temperatures from above and
57 below the OH layer into the computed temperature for that pressure level. Bearing in
58 mind that the OH profile is itself a broad layer \(FWHM ~8km\) and the rotational
59 temperatures computed correspond to a similar integration over the width of the layer it is
60 not unreasonable to compare OH with MLS temperatures. Indeed we find good
61 agreement.](#)

62

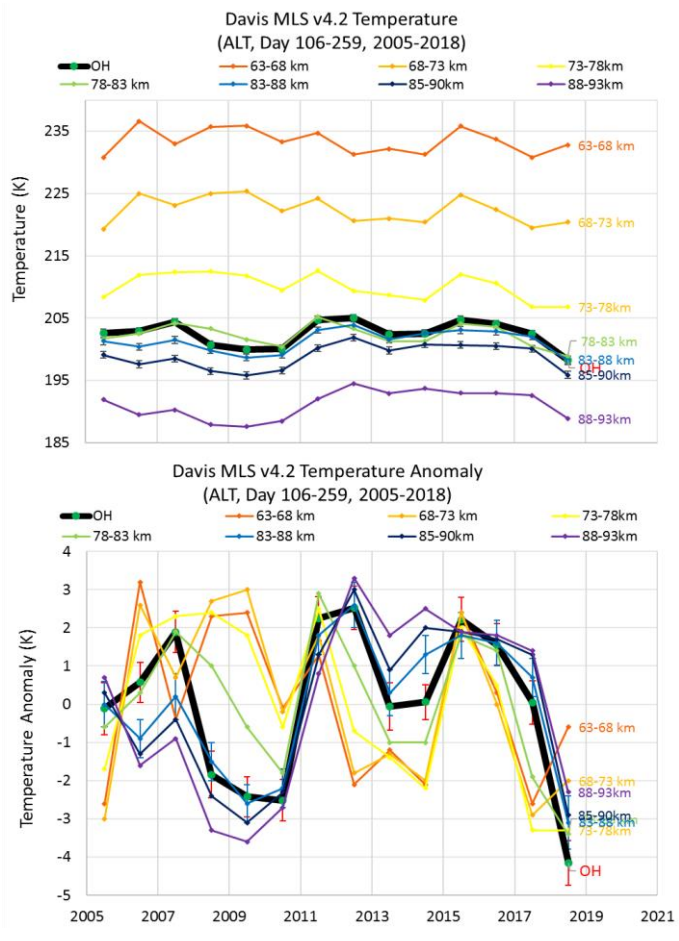
63 [We have previously reported, and routinely compare our measured OH temperatures with
64 both Aura/MLS and SABER profiles. In particular, French and Mulligan, 2010 examined
65 biases between Davis OH temperatures and both Aura/MLS and SABER. A significant
66 limitation of SABER for comparisons with Davis observations is the yaw cycle sampling
67 of the satellite. Comparable observations over Davis are confined to two intervals \(day-
68 of-year 75–140 and 196–262\) and days prior to 106 and after 259 are outside the OH
69 winter averaging interval. Therefore only days 106-140 and 195-259 are comparable and](#)

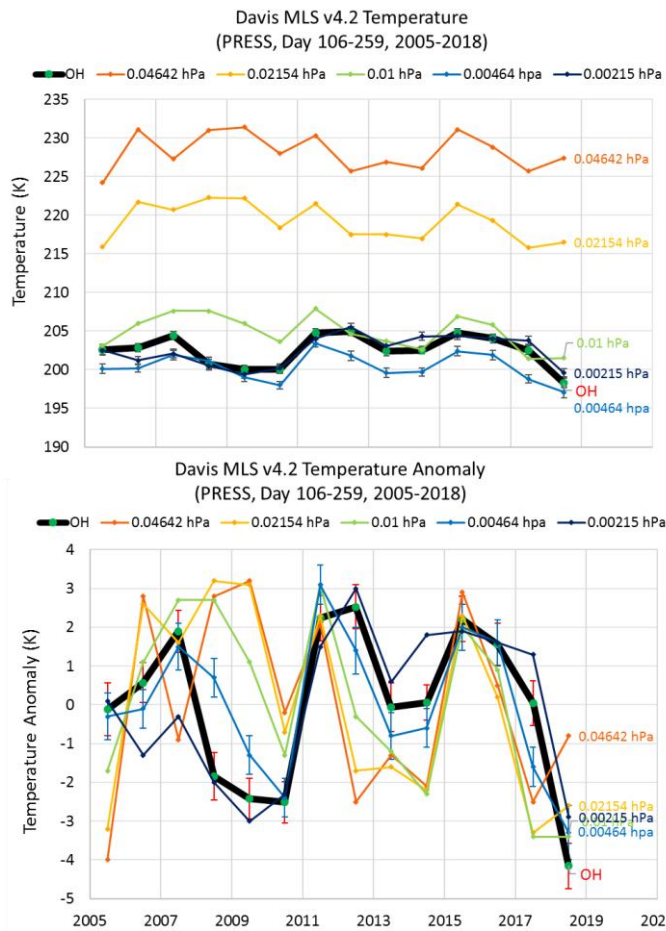
70 a large part of the winter months is not sampled. As a consequence SABER winter
71 averages do not fit the OH observations at Davis as well as MLS.

72
73 We agree that the geometrical altitude of the layer varies. Since the hydroxyl layer
74 position is primarily controlled by collisional quenching with O₂ and N₂ on the bottom-
75 side of the layer, and reaction with atomic oxygen on the top-side of the layer it is the
76 concentration (density) of the reacting species that governs the layer position. Therefore it
77 is reasonable to compare with MLS pressure (proportional to density) levels than on
78 geometrical altitude levels. See also details of SABER altitude and pressure plots
79 addresses in item 20 below.

80
81 This work is primarily concerned with mesopause region trends and absolute temperature
82 biases are removed by subtraction of the climatological mean. We work here with
83 anomalies (difference from the mean of all years) and residuals (solar cycle component
84 removed). In selecting the 0.0046hPa level we compared the Davis OH winter average
85 anomaly with MLS [AMJJAS average] anomaly over a range of altitude and pressure
86 levels. (see plots below, the first are altitude ranges, the second pressure levels, both
87 temperatures and the anomaly are shown).

88
89





91
 92
 93
 94
 95
 96
 97
 98
 99
 100
 101
 102
 103
 104
 105
 106
 107

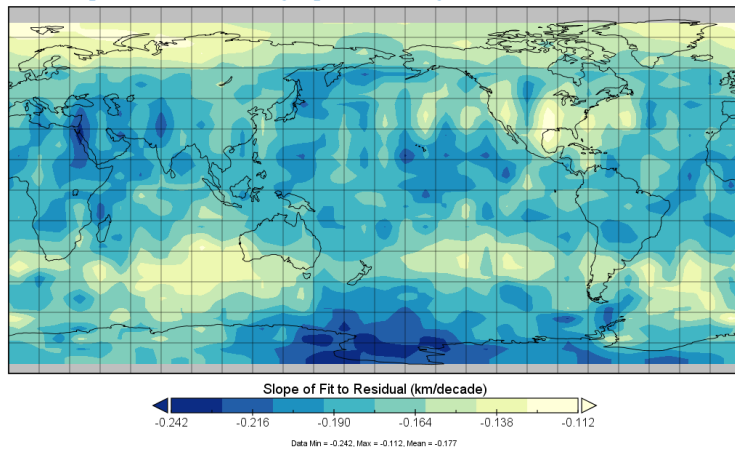
Altitude ranges 78-83km, 83-88km and 85-90km and pressure ranges 0.00215hPa and 0.00464hPa are all in reasonable agreement (<5K in absolute terms) with the OH temperatures, but we know there are biases with MLS (see French and Mulligan, 2010), and we know that the Davis OH temperatures are ~2 K high using LWR transition probabilities compared to those computed with the experimentally measured transition probability ratios determined in French et al 2000. These biases are removed by comparing anomalies. We calculate the Chi-Square goodness of fit parameter between the OH winter average anomaly with the Aura/MLS anomalies. The 0.0046hPa pressure level yields the smallest chi-sqr (14.8) compared to a layer centred on the traditional 87km altitude level (85-90km chisqr=18.8). This difference is small, but we prefer the pressure level comparison for the reason given above.

The relationship between pressure and geopotential height (GPH) is examined below using the MLS data set. Global decreases in GPH anomaly (between ~110 to 240

108 metres/decade) at the 0.0046hPa pressure level are consistent with a contraction of the
109 underlying atmosphere and also consistent with the SABER trend in OH mean winter
110 layer altitude for Davis shown in Fig 7. (200metres/decade) and discussed in the text.

111
112
113

MLS slope of fit to residual geopotential height at 0.0046hPa



114
115
116
117

118 There is also a lack of discussion on previously reported seasonal or latitudinal effects on
119 trends that the authors mention but do not connect with their results. It would be useful to
120 overplot these results from other authors on the corresponding figures in the manuscript.

121
122
123

We have modified figure 6 to indicate the solar cycle response and long-term trend coefficients available from other authors listed in Table 1.

124
125
126
127
128
129
130
131
132

A comparison of the seasonal variations in long-term trends has been previously published in a similar figure to Fig 5. in French and Klekociuk, 2011 (their figure 7; reproduced below). This included the results of Offermann et al 2010 at Wuppertal and Espy and Stegman (2002) from Stockholm. Since there has not been further updates to the seasonal variation in trend coefficients at either site we have not replicated this comparison. Perminov et al., 2018 offer seasonal variances in OH temperatures for the Russian sites of Zvenigorod and Tory but do not compute seasonal trend components.

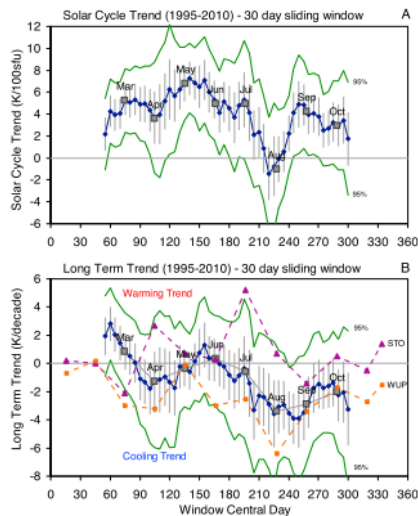


Figure 7. The 30 day sliding window (5 day step) evaluations of (a) solar cycle and (b) long-term trend coefficients at zero F10.7 lag (i.e., the vertical transect through Figure 6 (right-hand panels) at zero lag). One-sigma error bars and the 95% confidence limits (upper and lower traces) are as marked. The (true calendar) monthly evaluations are also plotted and labeled. Overlaid on Figure 7b are the equivalent monthly trend results by *Offermann et al.* [2010] from Wuppertal (labeled WUP) and *Espy and Stegman* [2002] from Stockholm (labeled STO). These are approximate values scaled off their respective seasonal trend plots and are offset by 6 months to match the Southern Hemisphere season.

133
 134
 135
 136
 137
 138
 139
 140
 141
 142
 143
 144
 145
 146
 147
 148
 149
 150
 151
 152
 153
 154
 155

The discussion section is too long. It is a good review but it is not easy to follow and, more importantly, to see how the results presented here fit on the discussion. I suggest revising the section, shortening it and putting the results of this paper into the context.

The discussion section has been substantially revised and some sections removed.

Other comments and suggestions are:

1. L42---45 Include in the abstract the result of the global MLS trend analysis.

We have included in the abstract the Aura/MLS solar cycle (3.39 ± 2.3 K/100 sfu) and long term trend (-1.3 ± 1.2 K/decade) coefficients at Davis for comparison. These are computed from anomalies derived from the AMJJAS means of all satellite observations within 500 km of Davis station over the 14 years of MLS observations (compared to 24 years of OH observations at Davis).

We note from Fig 6 that significant variability appears in both long term trend and solar cycle coefficients computed from MLS on a global scale. The global coefficients from MLS computed in the 5° latitude x 10° longitude grid boxes for AMJJAS averages at 0.0046hPa range from -2.3 to +2.3 K/decade (mean -0.01 K/dacade) for the long term

156 trend and -0.2 to 8.8 K/100 sfu (mean 3.3 K/100sfu) for the solar cycle. It is not practical
157 to include all the global MLS trend results in the abstract.

158

159 2. L148--L151. Is there any error associated to that interpolation?

160

161 Yes. The interpolation attempts to account for changes in the overall intensity of the OH
162 emission during the course of the 7 minute scan. In some cases the intensity may not vary
163 in a linear fashion, but in general interpolating intensities to a common time between
164 consecutive scans provides a better estimate for varying intensity of the OH emission.
165 Selection criteria limit extreme rates of change of intensities (<6%) between consecutive
166 spectra.

167

168 The error assigned to each line intensity is the square root of the total number of counts,
169 together with an error in estimating the background under each line. A standard deviation
170 error is also derived from the 3 different ratios contributing to the weighted mean
171 temperature for each pair of consecutive spectra. The process is described in detail in
172 French and Burns (2004) in sections 2. Measurements and 3. Rotational temperature
173 analysis.

174

175 French, W. J. R. and Burns, G. B.: (2004) "The influence of large-scale oscillations on
176 long-term trend assessment in hydroxyl temperatures over Davis, Antarctica", J. Atmos.
177 Sol. Terr. Phys., 66, 493–506. 634

178

179 3. L151. Is that 2% contribution independent of temperature? Or in other words, do
180 potential uncertainties in the Q--line contribution incur into significant errors in the
181 derived temperatures?

182

183 No, the $Q_1(5)$ is not temperature independent, but its contribution to $P_1(2)$ is computed in
184 an iterative process using the final weighted mean temperature from three possible ratios
185 from the $P_1(2)$, $P_1(4)$ and $P_1(5)$ lines. The contribution of the two lambda doubled
186 components of $Q_1(5)$ and computed separately from the final weighted mean temperature.
187 Approximately 98.0% of $Q_1(5)_e$ and 47.5% of $Q_1(5)_f$ contribute to the $P_1(2)$ emission
188 intensity we measure, depending on the instrument line shape measured via frequency
189 stabilised laser.

190

191 4. L157. Please, write a short sentence explaining why your choice is Langhoff et al. (1986).

192

193 We use Langhoff et al. (1986) transition probabilities because they are closest to the
194 experimentally measured, temperature independent line ratios determined for the OH(6-2)
195 band using the same instrument in French et al 2000.

196 Recent work by Noll et al ([https://www.atmos-chem-phys-discuss.net/acp-2019-](https://www.atmos-chem-phys-discuss.net/acp-2019-1102/acp-2019-1102.pdf)

197 [1102/acp-2019-1102.pdf](https://www.atmos-chem-phys-discuss.net/acp-2019-1102/acp-2019-1102.pdf)) also show relatively small errors in the comparison of

198 populations from P- and R- branch lines for the Langhoff et al (1986) coefficients, as well
199 as van der Loo and Groenenboom (2008) and Brooke et al. (2016) coefficients. The latter
200 two sets were not available at the time of that study.

201 The paragraph was modified to encompass this explanation.

202

203

204

205

206 5. Do you reach better agreement with satellites when using specific values?
207

208 This study is not an assessment of the bias between Davis OH temperatures derived with
209 different transition probabilities and satellite measurements. We have previously
210 examined this in French and Mulligan, 2010.
211

212 This work concentrates on the trends and variability inherent in the annual anomalies
213 (any bias is removed by subtraction of the climatological mean) and thus is independent
214 of the choice of transition probabilities (see further comments below). However, we do
215 obtain good agreement of absolute temperatures using Langhoff et al (1986) probabilities
216 (justified above) with Aura/MLS at the 0.0064hPa level and with SABER using a
217 Gaussian fit to the OH-B channel VER (French and Mulligan, 2010), given the many
218 assumptions made with regard to the layer height and shape, the width of the averaging
219 kernel used for satellite retrievals.
220

221 6. L160. Did you explicitly test the effect on trends of the probabilities used? How much is
222 "not significantly"? This is important in order to understand differences in trends
223 between the different datasets.
224

225 From the rotational temperature equation for the temperature derived from the ratio of
226 emission lines m and n

227

$$T_{rot} = \frac{E_m - E_n}{k \ln \left(\frac{I_n \cdot A_m \cdot (2J'_m + 1)}{I_m \cdot A_n \cdot (2J'_n + 1)} \right)}$$

228
229 Where E are the upper state energies, I are the measured intensities, A are the transition
230 probabilities, J' are the upper state rotational quantum numbers and k is Boltzmann's
231 constant.
232

233 Choice of a particular transition probability set only affects the ratio A_m/A_n and
234 corresponds to an offset in T_{rot} . While this choice is important for comparisons of
235 absolute temperature observations between sites, it is not important for studies of trends
236 and variability so long as the same transition probability set has been used consistently
237 for all years.
238

239 In this study, removal of the climatological mean, subtracts any offset due to differences
240 in the transition probability ratio. The only conceivable differences between the
241 temperatures derived using different sets is selection criteria boundary effects (whether
242 individual measurements pass selection criteria on the extrema of the selection criteria
243 limits). We believe (as for item 4 above) that Langhoff et al (1986) TP's are consistent
244 with the experimentally measured, temperature independent ratio's examined in French et
245 al 2000 and thus provide a reasonable estimate of the absolute temperature for
246 comparison with SABER, Aura MLS, and other observations, however we make no
247 assessment of bias against other observations here. Rather we assess trends and
248 variability in the anomalies.
249

249 The paragraph has been modified to express these points.
250
251

252 7. L161---163. This sentence is somehow redundant. If biases due to the choice of
253 probabilities can reach 12K, it is obvious that comparisons between different
254 instruments depend on the choice. Please, delete.

255
256 Deleted.

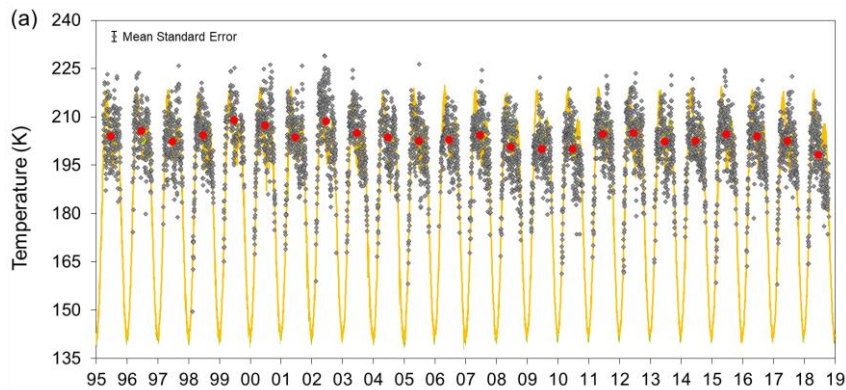
257
258 8. L169. Specify selection criteria quantitatively.

259
260 Paragraph modified to read “Selection criteria limit extreme values of weighted standard
261 deviation (< 20 K) and counting error (< 15 K), slope (< 0.06 counts/Å), magnitude (<
262 250 counts per second) and rate of change (< 3 counts per minute) of the backgrounds
263 and the rate of change of branch line intensities (< 6%) between consecutive scans.
264 Further details of the rotational temperature analysis procedure are available in Burns et
265 al. (2003) and French and Burns (2004)”

266
267
268 9. L183 and Fig. 1. There are more recent versions for MSISE. Use latest version or at least
269 show that it makes no difference.

270
271 Reference model updated to NRLMSISE-00. It makes little difference on the scale of the
272 plot in fig 1.

273



274
275 Fig1 caption modified accordingly and the reference updated to Picone et al 2002
276 [Picone, J. M., A. E. Hedin, D. P. Drob, and A. C. Aikin, NRLMSISE-00 empirical
277 model of the atmosphere: Statistical comparisons and scientific issues, J. Geophys. Res.,
278 107(A12), 1468, doi:10.1029/2002JA009430, 2002.]

279
280 The reference atmosphere (values for local midnight at Davis) has also been added to
281 Figure 2 for comparison and text added to discuss the differences.

282

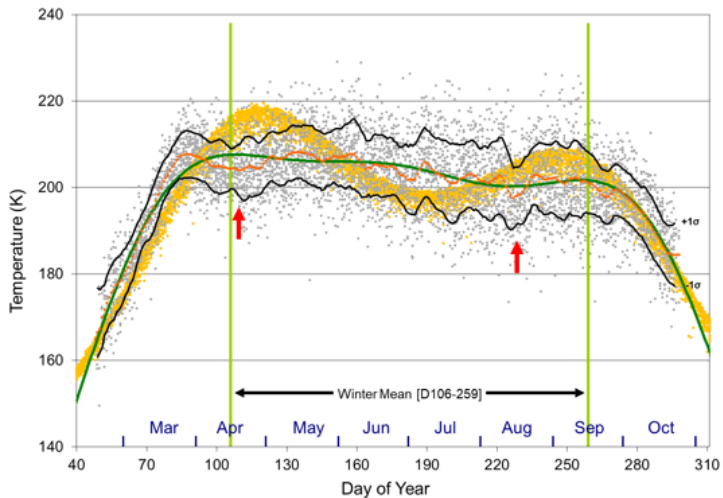


Figure 2. Superposed nightly mean temperatures from 1995 to 2018 [gray points] and a 5-day running mean which represents the climatological mean [orange line] with 1σ intervals [black lines]. The seasonal variation [green annual, semi-annual, ter-annual fit] and mid-April and mid-August dips [red arrows] are also indicated. Green vertical lines mark the calculation region for winter mean temperatures (inside the winter to summer transition intervals). The NRL-MSISE00 reference atmosphere (local midnight values for Davis) is also added for comparison [gold points]

283
284
285
286
287
288
289
290
291
292
293
294
295
296
297
298
299
300
301
302
303
304
305

10. L190. Introduce Fig. 2 at the beginning of this paragraph.

Inserted "(Fig. 2)" at the end of the first sentence and removed the sentence introducing Figure 2 midway through this paragraph.

11. L207---210. Remove this text from the caption. It is already in the text

Removed text and modified caption as for item 9 above.

12. L228. Are these MLS nightly means? Is there any time difference criterion used? If not, consider discussing possible sampling effects.

These are AMJJAS (6-month) means derived from all MLS observations within 500 km of Davis station as described in that line and in the paragraph from L282. There are only about 60 coincident samples per month (2 per night) within this range which gives little opportunity to apply a time restriction criterion.

Examination of nightly OH measurements show that tidal magnitudes are small (diurnal tide is $<2K$ and semidiurnal $<1K$) and averaging over 6 months, and with the vertical averaging kernel of MLS at this altitude will average out tidal effects.

306 13. L246---252 and Fig. 4. This is a very nice and colorful figure but is it really essential or a
307 short sentence would be enough?

308

309 It was considered that the histograms were useful to show the variability and skewness in
310 temperature distributions between years as a function of the mean annual winter
311 temperature. It would be difficult to describe the range of distributions displayed in a
312 short sentence.

313

314 14. L284. The choice of this altitude range sounds somehow arbitrary. The OH layer is not
315 centered at 85km. Please, justify. What happens if you use 85---90km?

316

317 The altitude range selected was not arbitrary, but as the altitude range of the smallest chi-
318 sqr fit to the OH temperatures. See discussion under first main comment.

319

320 15. L290. This is the main problem I see using MLS data for this study. Why don't you use
321 SABER data, even with a smaller time---coverage during the winter months? It could do
322 a good job in your 60---day running means solar and linear trends. Garcia---Comas et al.
323 (2014) showed that MLS biases at these altitudes could be large on the South Pole.

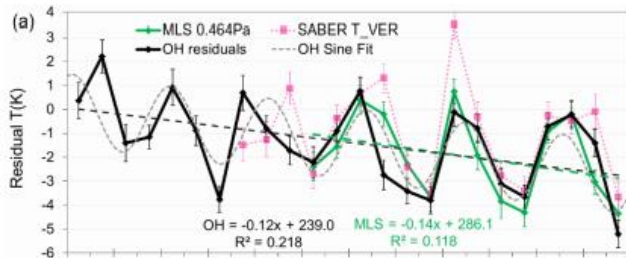
324

325 We include the equivalent curve for SABER data in Part 2 (Figure 1) of this work on the
326 QQO (available in discussions as acp-2019-1097). SABER's 60 day yaw cycle limits
327 comparable observations over Davis to two intervals (day-of-year 75--140 and 196--262)

328 and days prior to 106 and after 259 are outside the OH winter averaging interval.

329 Therefore only days 106-140 and 195-259 are comparable and a large part of the winter
330 months is not sampled. As a consequence SABER winter averages do not fit the OH
331 observations at Davis as well as MLS.

331



332

333

334

335

336 SABER data and results are discussed extensively in the discussion and used to in section
337 5.3 to assess trends in the change in the height of the OH layer.

338

339 16. L293. The choice of this pressure level is not justified. You could be getting a good
340 agreement due to a bias that could be masking a wrong selection of altitudes. Indeed, it
341 is well known that the altitude of the OH---layer is variable (as you even mention in
342 L582--584). Please, discuss this point.

343

344 We do not match absolute temperature but the variance in winter mean temperature
345 anomalies over 14 years. The 0.0046hPa pressure level is selected as it yields the smallest

345

346 chi-square of the pressure levels. See discussion above under main comments and item
347 20 below.

348

349

350 17. L299. Yes, you show this very nicely in Fig. 5, my favorite figure of the paper.

351

352 Yes, trends are not uniform, and the seasonal variation should be considered when
353 comparing trends between observers. This is why we attempt to present some insight into
354 seasonal and spatial trend variability of the mesopause region using the MLS dataset.

355

356 18. L302. Indicate the figure where this is shown.

357

358 Examination of the QQO feature is separated and undertaken in Part 2 of this work. The
359 paper became too unwieldy to include both the trends analysis and QQO investigation in
360 the one manuscript. This is brief statement on the seasonal variability of the QQO with
361 the following sentence indicating it is discussed in more detail in part 2. The figure is
362 provided as Figure 1b in Part 2. (reproduced below)

363

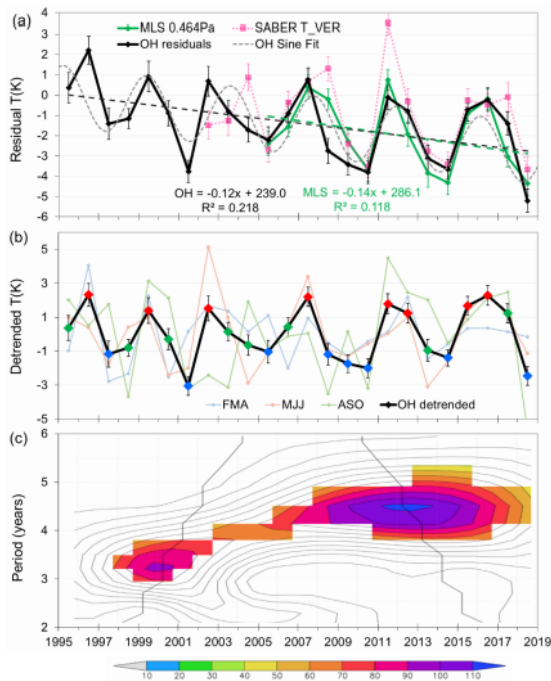


Figure 1. (a) Davis OH winter mean residual (solar response removed) temperatures (black line, standard error in mean error bars, dashed linear fit) compared with Aura/MLS [AMJJAS] mean residual temperatures for 0.0046 hPa (green line, standard error-in-mean error bars, dashed linear fit) and TIMED/SABER (pink dotted line, standard error-in-mean error bars). Gray dotted line is a sinusoid fit (peak-peak amplitude 3.0 K period 4.2 years). (b) Detrended Davis OH winter mean temperatures [AMJJAS] (black line, long-term linear fit removed) compared to FMA, MJJ and ASO monthly averages (red, green and blue points mark warm, mid and cold years for composite studies). (c) A Morlet wavelet transform (order 6) of the detrended Davis OH winter mean temperatures. Coloured sections are power significant above 90% level as per colour bar. The black line indicates the cone of influence; points outside have been influenced by the boundaries of the time series.

364
 365
 366
 367
 368
 369
 370
 371
 372
 373
 374
 375
 376
 377
 378
 379

19. L304. Aura/MLS trends "at 0.00464 hPa"

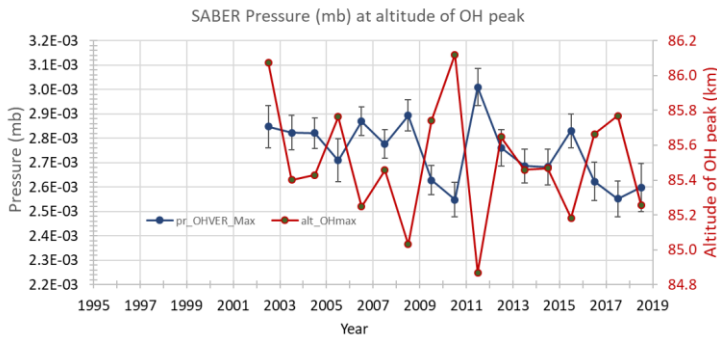
Text added as suggested

20. L307. How did you derive that this is the OH equivalent pressure level and that it does not change with latitude? Does SABER, measuring OH emission and temperature vs z and pressure, show a significant change of equivalent pressure with latitude?

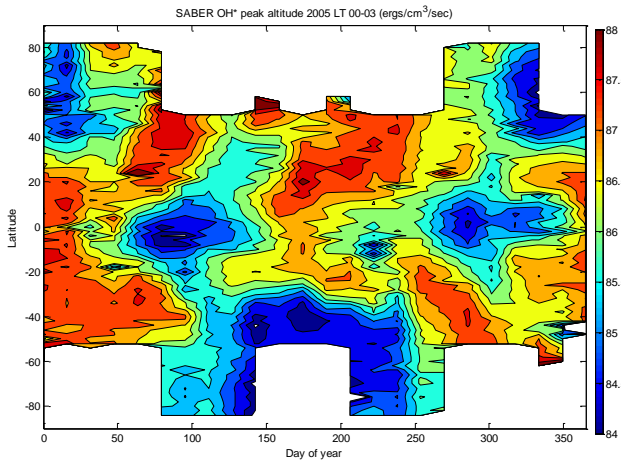
As discussed above at the variation of the [AMJJAS] anomaly had the smallest chi-sqr compared to the measured OH winter average temperature anomaly at Davis.

The Figure below shows a comparison of SABER VER (altitude of peak) and corresponding pressure value (mb) for the years 2002-2018 (day 106 – 259 of each year)

380 at Davis Station. The OH peak occurs at pressures in the range 0.00255 hPa to 0.003 hPa
 381 (2.55×10^{-3} - 3.0×10^{-3} mb). This value lies between two of the Aura MLS levels (0.00464
 382 hPa and 0.00215 hPa) on which the averaging kernels are centered and is in excellent
 383 agreement with the Davis MLS 4.2 Temperature PRES plot (page 3 above) included in
 384 response to the first Main Comment above. An inverse relationship between altitude and
 385 pressure at the OH peak is clearly evident, and justifies the selection of a pressure level
 386 comparison for OH temperatures over an altitude level.
 387
 388



389
 390
 391 On the question of the altitude (or pressure) of OH peak as a function of latitude, the
 392 figure below shows the variation of the altitude of the OH peak as a function of latitude
 393 and day-of-year for the year 2005 from SABER data. The overall pattern shown here is
 394 repeated year after year with only minor changes in detail.
 395



396
 397
 398 Based on the two figures above, the MLS averaging kernel centered on 0.00464 hPa
 399 would appear to be a good representative for the temperature of the OH layer.
 400

401
402 21. L308. Monthly anomalies? 60---night running means? What are these?
403
404 These are AMJJAS (southern hemisphere winter months) averages as described on L309.
405
406 22. L316. What is the origin of these enhance bands?
407
408 To the best of our knowledge, this is the first time that these bands have been reported.
409 This observation is discussed in the context of similar work (both observational and
410 modelling) in section 5.4.
411
412 23. Section 5.1. I enjoyed reading the review but it could probably be shortened and
413 better organized and your results should be put into the context you describe. Are
414 they reasonable? Do they agree? Does the seasonality of your data agree with other
415 results? Does it agree with the expected variations? I suggest extending the title of
416 this section in order to include ozone.
417
418 Section 5.1 subtitle was modified to include ozone.
419
420 Section 5.1 does compare the present results with other reports in their context, e.g., in
421 lines: 426-420, 459-460, 503-504, 510-511, 558-559 (line numbers refer to the original
422 manuscript).
423
424 We have significantly shortened (from 114 to 84 lines) and reorganised the discussion
425 in this section from line 427-487 – omitted the discussion of ACE-FTS CO₂ rates of
426 change and merged and modified the section from L436-477 to replace with the
427 following -
428
429 “In a recent summary of progress in trends in the upper atmosphere, Laštovička (2017)
430 identified greenhouse gases, particularly CO₂ as the primary driver of long-term trends
431 there. The overall effect of greenhouse gases at mesospheric altitudes is radiative
432 cooling. The important secondary trend drivers in the mesosphere and lower
433 thermosphere (MLT) are stratospheric ozone, water vapour concentration and
434 atmospheric dynamics. Temperature trends are predominantly negative, and recent
435 progress in understanding the magnitude of the cooling have arisen from confirmation
436 and quantification of the role of ozone. Lübken et al. (2013) present the results of
437 trend studies in the mesosphere in the period 1961-2009 from the Leibniz-Institute
438 Middle Atmosphere (LIMA) chemistry-transport model which is driven with European
439 Centre for Medium–Range Weather Forecasts (ECMWF) reanalysis below 40 km, and
440 observed variations of CO₂ and O₃. They find that CO₂ is the main driver of
441 temperature change in the mesosphere, with O₃ contributing approximately one third to
442 the trend. Linear temperature trends were found to vary substantially depending on the
443 time period chosen primarily due to the influence of the complicated temporal variation
444 of ozone.
445
446 Figure 3 of (Lübken et al., 2013) show a monotonically increasing trend on CO₂
447 compared with a much more complicated temporal ozone variation (essentially
448 constant until 1980, a rapid decrease from 1980-1995, followed by an increase since
449 then. Trends in ozone vary as a function of both altitude and latitude, with positive
450 trends dominating in the lower stratosphere and mesosphere. Increases in water vapour

451 concentration are considered a secondary but non-negligible effect particularly in the
452 lower thermosphere (Akmaev et al. 2006). The trend effect of dynamics was found to
453 be very slightly negative in the mesosphere, but very small compared with the
454 radiatively induced trends. At the mesopause, the trend due to dynamics was positive
455 and significantly larger (~1 K/decade). These results were found to be in good
456 agreement with observations from lidars, Stratospheric Sounding Units (SSU) (Randall
457 et al., 2009) and radio reflection heights which have decreased by more than 1 km in
458 the last 50 years due to shrinking in the stratosphere/lower mesosphere caused by
459 cooling.”
460
461 The paragraph from lines 478-486 had also been omitted.
462
463 24. L440. Include reference.
464 25. L449. Include reference.
465 The reference for both lines is Laštovička (2017), which appears in the opening line of
466 the paragraph containing those lines. The reference was included again at the end of the
467 (modified) paragraph.
468
469 26. L465. This is already said, also mentioning the same reference.
470 Replaced with the modified paragraph as above (Item 23).
471
472 27. L478---486. It is not clear to me what this has to do with this work. Hervig et al. (2019)
473 paper mainly deals with the paradox on the solar response of H2O. Perhaps mentioning
474 only their result related to temperature makes more sense. By the way, do you actually
475 see a change of solar response of temperature from 1995 to 2018?
476
477 The Hervig et al (2019) reference and following discussion has been omitted in the
478 revision of section 5.1.
479
480 The period 1995-2018 spans only 2 solar cycles, assessing the response of the two cycles
481 independently would not be constructive considering the uncertainties.
482
483 28. L488. Also Solomon et al. 2018
484
485 The work of Solomon et al. (2018) using WACCM-X is cited in lines 662-671. The two
486 studies are discussed separately, since Solomon et al. use constant low solar activity
487 conditions in an attempt to disentangle temperature changes arising from anthropogenic
488 effects from solar induced variations.
489
490 29. L501---502 I do not understand "global averaged temperature (..) as a function of
491 latitude". How does their month---to---month variability compare with the seasonal
492 variability you derive? Please, overplot on Fig. 5 and discuss.
493
494 Corrected “.. zonal average ..”. Sentence now reads “ Qian et al. (2019) provide zonal
495 averaged temperature trend values as a function of altitude (50-110 km) and latitude for
496 each month (their Fig. 3) some of which are statistically significant.”
497
498 30. L507. Please, write altitude
499 The word altitude *is* present in the sentence.
500

501 31. L559. Write "from 1995 to 2018". If you remove your QO, don't you see such breaks?
502 From your measurements, it seems that your trend is not monotonic. Quantify "no
503 obvious sign".

504
505 Added "from 1995-2018" to the end of the sentence.

506
507 We are not certain how you propose we remove the QO variation. In order that it be
508 removed the process generating the QO needs to be understood. We devote significant
509 effort to examine this QO signal in more detail in Part 2 of this work but are unable at
510 this stage to isolate the mechanism, therefore have no index to model the QO.

511
512 If there was a trend break in the period 1995-2018, one might expect to see a significant
513 change in the trend, and in the solar response, when extending the period of the study
514 from 16 years to 24 years. Such a change is not observed (as you note in your opening
515 paragraph "the trends derived here coincide with their previous results and those for the
516 solar response are only slightly different"). To quantify, the coefficients over

517 16 years (French and Klekociuk, 2011) were

518 4.30 ± 1.02 K/100sfu (95% confidence limits 2.2 K/100sfu $< S < 6.4$ K/100sfu)

519 -1.20 ± 0.51 K/decade (95% confidence limits -0.14 K/decade $< L < -2.26$)

520 and 24 years were

521 4.79 ± 1.02 K/100sfu (95% confidence limits 2.6 K/100sfu $< S < 6.99$ K/100sfu)

522 -1.18 ± 0.87 K/decade (95% confidence limits 0.71 K/decade $< L < -3.06$)

523 Neither coefficient has changed outside the uncertainty.

524
525 We are unsure how you deduce from our measurements that the "trend is not
526 monotonic"?

527
528 32. L584. Please, also mention Liu et al. (2006).

529
530 Added Liu et al. (2006).

531
532 33. L592. Garcia---Comas et al. (2017) also estimated the trend and solar response of OH*
533 altitude and temperature from SABER.

534
535 The following sentence has been added after line 580. "García-Comas et al. (2017)
536 reported a slightly larger decrease of 40 m/decade in SABER OH volume emission rate
537 weighted altitude at mid-latitudes which accompanied a 0.7%/decade increase in OH
538 intensity and a 0.6K/decade decrease in OH equivalent temperature."

539
540 34. P610. What is the expected change in MLS temperatures due to a change of 0.02---0.04
541 km? This may lead to a bias in the comparison between DAVIS and MLS. A way to test
542 this could be done with SABER data by comparing temperature trends at a fixed altitude
543 to temperature trends at a OH VER weighted temperature.

544
545 Since the averaging kernel of MLS temperatures at the OH altitude is of the order of
546 15km a change of 20 to 40 metres over 16 years (determined from SABER VER altitude
547 2002-2018, shown in Fig 7) is negligible!.

548
549 35. L657---661 Why are these results so different? Could the difference be due to sampling?

550

551 WACCM-X is a model, Aura/MLS is measured data. The overall long term trend in
 552 WACCM-X at 85km is -0.52 ± 0.64 K/decade (Fig 10 in Qian et al., 2019) although
 553 zonally averaged monthly trends are more variable (Fig 3 in Qian et al., 2019).

554
 555 36. L720. According to a possible contribution of 30% by ozone, these values have (at least)
 556 a 30% error.
 557

558 The clause in parenthesis in lines 721-722 acknowledges the fact that the trend quoted
 559 ignores possible contributions of stratospheric ozone to the trend.

560
 561 37. L723---726. Could you provide the reason for this minimum in 2009?

562
 563 The minimum of both the solar cycle and QO cycle occur in 2009. (See Fig 3a.)

564
 565 38. L747. Mention here also the results from other OH observations (those listed in Table 1).

566
 567 We have re-written these sections with the request to shorten the discussion in section 5.
 568 Trend comparisons with other ground based observers listed in Table 1 is covered in
 569 section 4.4

570
 571 39. Fig1b. Do all years contain the same days of measurements from day 106 to 259? If not,
 572 there could be a sample bias.

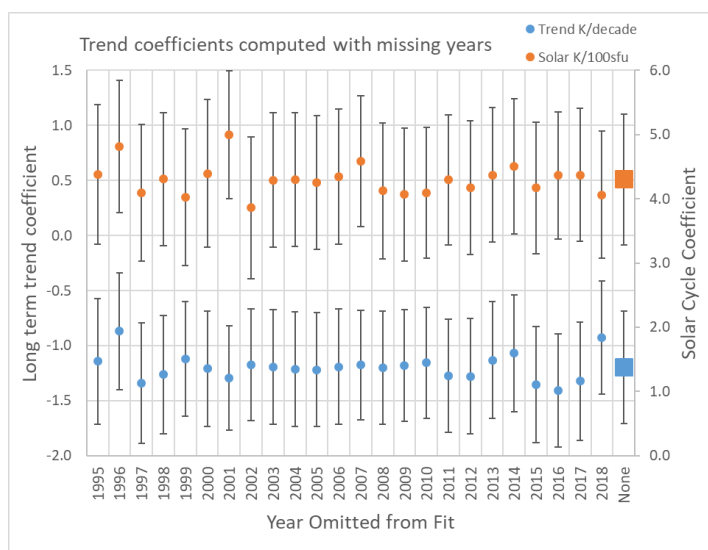
573
 574 With the exception of 1999 when 2 intervals D095-126 and 213-249 were used to scan
 575 the OH(8-3) band and 1996 missing D176-202 all other years only have more than 85%
 576 nights
 577 within the winter averaging window sampled. (ie 85% of the nights have a valid nightly
 578 average temperature with at least 10 measurements that pass selection criteria). A sample
 579 bias could be introduced in computing the anomalies if there was a significant departure
 580 from the climatological mean in those intervals.

581
 582

year	1995	1996	1997	1998	1999	2000
of 153	133	111	131	151	81	145
% nights	86.9%	72.5%	85.6%	98.7%	52.9%	94.8%
year	2001	2002	2003	2004	2005	2006
of 153	148	149	138	133	130	139
% nights	96.7%	97.4%	90.2%	86.9%	85.0%	90.8%
year	2007	2008	2009	2010	2011	2012
of 153	146	143	146	137	150	150
% nights	95.4%	93.5%	95.4%	89.5%	98.0%	98.0%
year	2013	2014	2015	2016	2017	2018
of 153	146	149	142	152	150	142
% nights	95.4%	97.4%	92.8%	99.3%	98.0%	92.8%

583
 584
 585 The sliding window (seasonal variation in trend parameters) give some indication of the
 586 range of trends obtained by selecting different intervals compared to the winter mean
 587 interval.
 588

589 We have also tested the effect on the derived coefficients by omitting individual years
 590 sequentially from the model fit computation. These show the range of coefficients if a
 591 data gap for the entire winter interval was missing. All coefficients derived from the
 592 omitted year computations remain within the uncertainty limits of the solar cycle and
 593 long-term trend coefficients when all years are included.
 594



595
 596
 597 The following paragraph was added to section 4.1 to address this concern
 598 “The stability of trend coefficients was tested for the presence of sampling gaps in the
 599 OH temperature record. With the exception of 1999 when 2 intervals D095-126 and 213-
 600 249 were used to scan the OH(8-3) band and 1996 missing D176-202 all other years only
 601 have more than 85% nights within the winter averaging window sampled. (ie 85% of the
 602 nights have a valid nightly average temperature with at least 10 measurements that pass
 603 selection criteria). A sample bias could be introduced in computing the anomalies if there
 604 was a significant departure from the climatological mean in those intervals. The test
 605 examined the effect on the derived coefficients by omitting individual years sequentially
 606 from the model fit computation. These show the range of L and S coefficients if a data
 607 gap for the entire winter interval was missing in a particular year. All coefficients derived
 608 from the omitted year computations remained within the uncertainty limits of the solar
 609 cycle and long-term trend coefficients when all years were included. “

610 40. Figure 2. Time coverage changes with doy. What is the effect of DW1?

611
 612
 613 Over the winter averaging window (D106-259) the diurnal time coverage varies from
 614 13:13 hrs (D106, 15-Apr) to 19:00 hrs (D177, 21-Jun) and 10:45 hrs (D259, 15-Sep).
 615 From the OH nightly observations we observe that the amplitude of the diurnal tide is
 616 <2K and semidiurnal tide <1 K.
 617

618 We sample the same hours on the same days each year, and average those over days 106-
 619 259 each year to derive the trends.

620
621 41. Fig 5.a. the minimum in solar trend is during the month when downwelling is maximum.
622 This might be an indirect compensation of the cooling due to the direct dependence of
623 downwelling (warming) and solar flux (COMPROBAR!!!)
624
625 We agree that the (August) minimum in the solar trend may indeed be the result of
626 indirect compensation of cooling by the warming from maximum downwelling at that
627 time of the year. However, we consider that removal of the climatological mean
628 calculated over two full solar cycles is the best that we can do to eliminate the substantial
629 part of the seasonal trend, leaving the anomaly values as shown in Figure 1(b). The solar
630 cycle and long-term trends were calculated simultaneously using linear regression on the
631 anomaly. A non-linear effect of the seasonal behaviour of the OH layer on the solar cycle
632 response, e.g., through downwelling of atomic oxygen rich air, which could lead to
633 increase production of CO cannot be ruled out, but is beyond the scope of the present
634 work.
635
636 42. Fig 5b. Perhaps you might be sounding different altitudes? What is the seasonal change
637 of the altitude of the OH layer? Did you look at SABER data? Also, this might be
638 connected to O3 trend seasonality or CO2 trend seasonality.
639
640 The altitude of the OH layer peak appears to have a substantial seasonal response at
641 DAVIS with an altitude minimum in mid-winter. However, we believe that removal of
642 the climatological mean over two full solar cycles together with fitting solar cycle and
643 long-term trends simultaneously would take account of this variation. Part 2 of this work
644 examines the seasonal and long-term relationships between observed trends
645 in temperature, CO₂, O₃, and CO.
646
647 43. Figure 5. Define grey boxes and blue dots.
648
649 These *are* defined in the figure caption.
650
651 44. Figure 6. What is time sampling for MLS? Are you removing tides? Trends strongly
652 depend on sampling (Rezac et al. 2018)
653
654 These are 6 month anomaly averages (AMJJAS and ONDJFM) in each grid box, as
655 described in the caption. They are the same averaging intervals each year. Tides are small
656 and average out over 6-month means.
657
658 45. Fig 6. Please, overplot trend at Davis on the 1d plot. Also indicate CAP and LEO position
659 on the maps.
660
661 Have modified figure 6 to indicate the positions of all ground-based observations in table
662 1 where long-term trend and solar cycle coefficients have been provided for comparison.
663 Note that the 1d plots are a zonal mean, and as the map plots show there is considerable
664 spatial variability in the trends derived from MLS data.
665
666
667 46. Fig 6. b. The blue/red bands at 70N in the NH winter months look like the trend and
668 solar response related to stationary PWs.
669

670 We are grateful for this interesting suggestion. In the interest of keeping the manuscript
671 to a reasonable length, we decided to defer a detailed study of this point, and we are
672 reluctant to speculate on it without supporting evidence.

673

674 47. Fig. 7. What is the relationship between this plot and the temperature anomaly? Can it
675 help to explain differences between DAVIS and MLS?

676

677 Section 5.3 describes the effect that a vertical shift in the altitude of the OH layer would
678 have on the emission weighted temperature which is measured by a ground-based
679 instrument like that at Davis. The purpose of Fig. 7 is to show that SABER data does not
680 indicate a significant change in the altitude of the OH layer during the period 2002-2018.
681 Therefore we can eliminate change in the altitude of the OH layer as a cause of
682 temperature change detected by the spectrometer at Davis.

683

684 This Figure does not address any differences between Davis and MLS.

685

686 48. Table 1. Discuss these results in the text, particularly mention them in section 5.

687

688 The majority of these results are discussed in the text in section 4.4. Section 5 has been
689 substantially re-written. See response to point 38 above.

690

691 49. Table 1. Include MLS results in this list

692

693 This table was constructed on the basis of ground-based measurements only (as described
694 in the caption), with the result that Aura/MLS results are not included. The global results
695 of MLS are provided in Figure 6.

696

697 Response to RC2

698 Interactive comment on “Analysis of 24 years of mesopause region OH rotational
699 temperature observations at Davis, Antarctica – Part 1: Long-term trends” by W. John R.
700 French et al. Anonymous Referee #1 Received and published: 7 February 2020
701

702 Reviewer Report on the manuscript acp-2019-1001 Analysis of 24 years of mesopause
703 region OH rotational temperature observations at Davis, Antarctica – Part 1: Long-term
704 trends by W. John R. French et al.
705

706 General Remarks

707

708 1. . . The paper presents 24 years of observations of OH temperatures, which is an
709 interesting extension of an earlier data set worth publishing.
710

711 [Thank you.](#)

712

713 2 The data were taken in Antarctica where such measurements cannot be performed in
714 summer. This is a drawback for several interpretation aspects and must be carefully
715 considered.
716

717 [Observations of the hydroxyl nightglow cannot be made over the summer at this latitude
718 and we understand this is a limitation of the observational program for long-term trends
719 using this technique. We contribute a solar and long-term trend assessment of the mean
720 winter temperatures at this high southern latitude site and make comparisons with
721 satellite observations to place these observations into global context.](#)
722

723 3 The data are discussed in the context of increasing CO₂ mixing ratios. They are
724 extensively compared to MLS and SABER satellite results, and to computer models
725 (WACCM-X).
726

727 [Yes, comparison with other observations and models place these measurements into
728 context.](#)

729

730 4 The paper gives a long term analysis and discusses possible trend breaks. These results
731 are questionable because of the lack of winter data.
732

733 [Winter data is provided. It is the southern hemisphere *summer* data that is lacking. We
734 make this clear from the outset of the manuscript.](#)
735

736 5 The authors see a quasi-quadrennial oscillation (QOO) in their data. They announce a
737 detailed discussion in a second part of the paper. This should take into account recent
738 work in the literature on 3 – 5 year oscillations.
739

740 [The second part of this work is available in discussions as acp-2019-1097](#)

741

742 6 The paper is well written, and is recommended for publication after some modifications.
743

744 [Thank you.](#)

745 Major Comments

746

747 Line 221 pp: Figure 3 indicates five oscillation periods. The approximate period lengths
748 are 2x 3 yr, 1x 4 yr, and 2x 5 yr. It is not obvious that a mean can be taken. Superposition
749 of a 3 yr and a 5 yr oscillation should be checked (see for instance Offermann et al.,
750 JASTP 135,1, 2015).

751

752 The quasi-quadrennial periodicity revealed in the residual temperatures (seasonal, solar
753 cycle and long-term trend fits removed) is an interesting feature and forms the basis of
754 part 2 of this work; available in discussions as [acp-2019-1097](#). We examine many
755 possible sources for this feature using correlation and composite analyses with other data
756 sets. We cannot ascertain whether the oscillation is a superposition of 3 and 5 year
757 periodicities.

758

759 Line 383 pp, 540: The paper Offermann et al., 2006, should not be used to demonstrate a
760 trend break. It was outdated by Offermann et al., JGR 115, D18127, 2010, who show a
761 longer data series.

762

763 The reference to Offermann et al., 2006 applied to a time period when trend breaks first
764 began to appear in the literature in relation to mesopause region temperature trends. In
765 that context the reference is still valid despite it being later updated. We have added the
766 updated reference (Offermann et al., 2010) to the paragraph noting the continued
767 occurrence of trend breaks.

768

769 Offermann, D., P. Hoffmann, P. Knieling, R. Koppmann, J. Oberheide, and W. Steinbrecht (2010), Long-term trends
770 and solar cycle variations of mesospheric temperature and dynamics, J. Geophys. Res., 115, D18127,
771 doi:10.1029/2009JD013363

772

773 Line 405 pp, Section 5.1, 5.4: In the discussion of the trend data it should be elaborated
774 that the summer data at Davis are missing. Trend data are different in summer and winter
775 as shown by the MLS data in your Fig. 6. They can also vary from month to month as
776 shown in your Fig. 5, but variations could be much larger (see for instance Offermann et
777 al., 2010, their Fig.9). Possibly the summer trends are larger than your 1.2 K/decade (by
778 number), and so might be the trend of annual data. Hence, if you want to include Davis
779 data to Tab.1 please use annual MLS data!

780

781 The fact that we derive a trend in the mean *winter* temperatures is explicitly stated in the
782 first sentence of the discussion in section 5.1 (lines 407-408) and in the first sentence of
783 section 5.4 (line 619) “southern hemisphere (SH) *winter* months (AMJJAS)”. We think it
784 should be clear to the reader that hydroxyl temperatures at Davis cannot be obtained over
785 the summer months as the sun does not go down.

786

787 We do explore the seasonal variation in trends where possible over the observing season
788 at Davis (fig 5) and understand that the trends are variable.

789

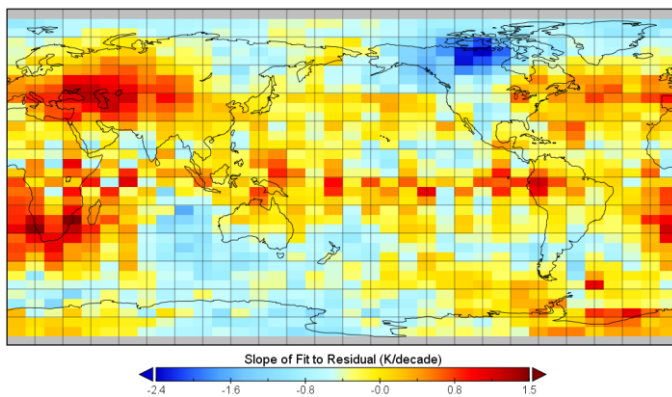
790 We also compare with MLS over winter and summer for each hemisphere (Figure 6) to
791 show the seasonal difference in trends. MLS does not indicate that the summer trends
792 [ONDJFM average trend plots in Fig 6] are larger than -1.2 K/decade for the grid box
793 over Davis. The grid box over Davis yields a long-term trend of $+0.02 \pm 0.08$ K/decade for
794 the summer months [ONDJFM] and an annual average value [JFMAMJJASOND] of -
795 0.37 ± 0.06 K/decade.

796 Table 1 is a list of ground based observations. It does not contain the MLS trends as they
797 are globally and seasonally variable. Figure 6 shows the map of these coefficients for
798 comparison with the ground based observations in Table 1.
799

800 Line 558/559: . . .”no . . .sign of a discontinuity in the trend. . .” Kalicinsky et al., 2018,
801 in their long-term analysis find that the summer data may be much more important than
802 the winter data. Therefore please check your above statement by means of annual MLS
803 data.
804

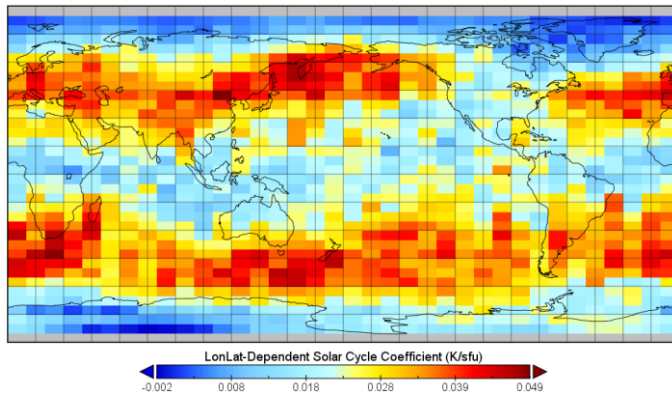
805 MLS values for the summer and winter seasons for each hemisphere are shown in Figure
806 6. It does not appear that the summer values are greater than winter values for the MLS
807 trend coefficients globally (the two linear trend plots in figure 6 use the same colorbar
808 scale). Coefficients maps (linear trend and solar cycle) for the whole year (all month
809 MLS averages) are provided below for comparison with those in Fig 6. It merges the
810 winter and summer features (as one would expect) and particularly highlights the mid-
811 latitude maxima in solar cycle response.
812

813 MLS Linear trend coefficient [JFMAMJJASOND]



814
815
816

MLS Solar cycle coefficient [JFMAMJJASOND]



817
818

819 Minor Comments

820

821 Line 219: The error of your solar cycle response (1.02 K/100sfu) appears relatively large
822 (see Tab.1). Do you know a reason?

823

824 The solar cycle response error is not unreasonably large compared to others in Table 1.
825 (less than, or of the same order as 7 out of 11). We would suggest that the main reason for
826 the error is the goodness-of-fit of the F10.7 and linear trend model. In particular that the
827 model does not contain a quasi-quadrennial oscillation term that is evident in the
828 residuals.

829

830 Line 295: Please give the error of the MLS trend.

831

832 MLS trend is 1.4 ± 1.1 K/decade . added to text

833

834 Line 325 pp, Fig.6: a) Please show Panel numbers. b) Please show latitude scales. c) Part
835 of the captions are difficult to read. d) Line 334: There is no Fig.1B. Do you mean
836 Fig.3b?

837

838 Added panel numbers and latitude scales and modified the figure to improve readability.
839 Yes, thank you we mean figure 3b for the comparison, but the caption has changed with
840 the addition of all sites to the map for comparison as requested by another reviewer.

841

842 Line 353 pp, Table 1: Please give the selection criteria for the sires shown.

843

844 We have updated the table from Table 2 in French and Klekociuk (2011) where updates
845 were available since 2011.

846

847 Line 456 pp: “. . . peak altitudes..” Here and in the following it is sometimes unclear
848 whether you mean the maximum of the peak or the geometric altitude. Please clarify.

849

850 We mean the altitude of the peak of the VER profile. This section has been extensively
851 modified in response to another reviewer and this paragraph is no longer included.

852

853 Line 505 pp, 508: It is unclear whether you mean your Fig.5 or Qian et al.. Please
854 clarify.

855

856 This refers to the seasonal variation in the solar cycle coefficient in our Fig 5(a) and can
857 be compared with Fig 4 of Qian et al (2019); this is clarified in the text.

858

859 Line 686: Fig.1a does not show this! Do you mean that you derived it from this Figure?

860

861 The R^2 value is shown in Fig 3(a) (Fit of solar cycle and long-term trend model to OH
862 temperatures). This is corrected in the text.

863

864 Line 693: Sentence difficult to understand.

865

866 Modified sentence to read “Although the altitude of the mesospheric cold point changes
867 with season (e.g., Yuan et al., 2019) and tends to be higher than the centroid height of the
868 OH* layer, the global solar response value obtained for T-CPM (4.89 ± 0.67 K/100 SFU)

869 is in good agreement with the solar response coefficient derived from ground-based OH*
870 observations.”

871

872 Line 706 pp: Where can this be seen? The Supplementary Material was not available to
873 me.

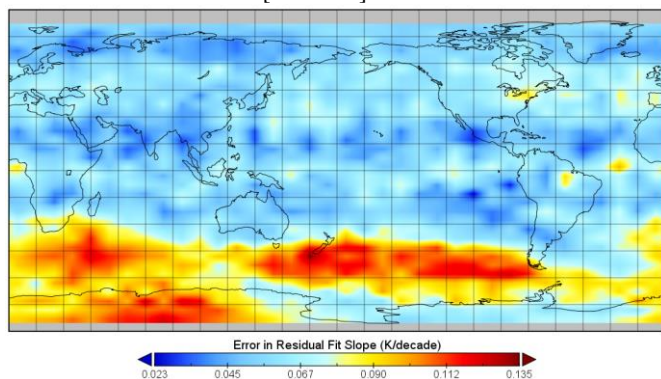
874

875 The original Fig 6. also contained a plot of the error in fitting the solar cycle and long
876 term linear trend model (see below) and the point was made here that where the error was
877 largest coincides with a strong QOO signal. However the QOO investigation is now
878 discussed entirely in Part 2 of this work (acp-2019-1097).

879 The paragraph was modified to read “As a final comment on the global trends, it is noted
880 that the largest errors in the linear trend fit for the SH winter understandably occur
881 coincident with the regions positively or negatively correlated with the QOO (not shown
882 here). The fit can be significantly improved if the QOO component can be understood
883 and modelled. We investigate the QOO in detail in part 2 of this work. “

884

885 Error in model fit to MLS [AMJJAS]



886

887

888

889

890

891

892 Tracked Changes Manuscript

893

894 Analysis of 24 years of mesopause region OH rotational temperature
895 observations at Davis, Antarctica. Part 1: Long-term trends.

896

897 W. John R. French¹, Frank J. Mulligan², and Andrew R. Klekociuk^{1,3}

898

899 ¹Australian Antarctic Division, 203 Channel Hwy, Kingston, Tasmania, 7050, Australia

900 ²Maynooth University, Maynooth, Co. Kildare, Ireland

901 ³Department of Physics, University of Adelaide, Adelaide, 5005, Australia

902

903 *Correspondence to:* W. John R. French (john.french@aad.gov.au)

904

905

906

907

908

909

910

911

912

913

914

915

916

917

918 **Abstract**

919 The long term trend, solar cycle response and residual variability in 24 years of
920 hydroxyl nightglow rotational temperatures above Davis Research Station, Antarctica (68°
921 S, 78° E) is reported. Hydroxyl rotational temperatures are a layer-weighted proxy for
922 kinetic temperatures near 87 km altitude and have been used for many decades to monitor
923 trends in the mesopause region in response to increasing greenhouse gas emissions.
924 Routine observations of the OH(6-2) band P-branch emission lines using a scanning
925 spectrometer at Davis station have been made continuously over each winter season since
926 1995. Significant outcomes of this most recent analysis update are (a) a record low winter-
927 average temperature of 198.3 K is obtained for 2018 (1.7 K below previous low in 2009)
928 (b) a long term cooling trend of $-1.2 \pm 0.51 \pm 0.2$ K/decade persists, coupled with a solar cycle
929 response of 4.3 ± 1.02 K/100 solar flux units and (c) we find evidence in the residual winter
930 mean temperatures of an oscillation on a quasi-quadrennial (QOO) timescale which is
931 investigated in detail in part 2 of this work.

932 Our observations and trend analyses are compared with satellite measurements
933 from Aura/MLS version v4.2 level 2 data over the last 14 years and we find close agreement
934 (a best fit [to temperature anomalies](#)) with the 0.00464 hPa pressure level values. The solar
935 cycle response (3.4 ± 2.3 -K/100sfu), long-term trend (-1.3 ± 1.2 K/decade) and underlying
936 QOO residuals [in Aura/MLS](#) are consistent with the Davis observations. Consequently,
937 we extend the Aura/MLS trend analysis to provide a global view of solar response and long
938 term trend for southern and northern hemisphere winter seasons [at the 0.00464 hPa pressure](#)
939 [level](#) to compare with other observers and models.

940

941

942

943 1. Introduction

944 Long-term monitoring of basic atmospheric parameters is fundamentally important
945 to understand natural, periodic and episodic variability in atmospheric processes, to provide
946 data to verify increasingly sophisticated atmospheric models and to resolve and quantify
947 perturbations due to global change on decadal to century timescales. Dynamical processes,
948 including gravity waves, tides, planetary waves, large scale circulation patterns and quasi-
949 periodic teleconnections (such as the quasi-biennial oscillation (QBO), El Niño Southern
950 Oscillation (ENSO), and the Pacific Decadal Oscillation (PDO)), changes to the chemical
951 composition and radiative balance (particularly due to anthropogenic emissions of
952 greenhouse and chlorofluorocarbon gasses) and external forcing such as the 27-day solar
953 rotation and 11-year solar activity cycle, all play significant roles (directly and through
954 interactions) in defining and perturbing the mean state of the atmosphere. Decades of well
955 calibrated measurements are required to accurately quantify variations and trends on these
956 timescales.

957 Meteorological reanalyses derived from assimilation of a vast number of surface
958 observations provide time-series for useful trend analyses ~~for~~in the lower atmosphere e.g.
959 (Bengtsson et al., 2004). A few satellite based data sets are now also reaching multi-decadal
960 timescales (e.g. the Thermosphere Ionosphere Mesosphere Energetics Dynamics satellite's
961 Sounding of the Atmosphere using Broadband Emission Radiometry instrument (TIMED
962 /SABER) (Mertens et al., 2003), and the Earth Observing System satellite Aura Microwave
963 Limb Sounder (Aura/MLS) (Schwartz et al., 2008), that extend observations to the upper
964 atmosphere. Of current and particular interest to climate science in the modern era are the
965 atmospheric temperature trends in response to increasing global greenhouse gas emissions,
966 principally from carbon dioxide (CO₂). Modelling studies over many years suggest that
967 the sensitivity to CO₂ changes in the upper atmosphere, particularly at high latitudes, is

968 much larger than in the lower atmosphere (e.g. Roble (2000), the Canadian Middle
969 Atmosphere Model (CMAM) (Fomichev et al., 2007)) and the Hamburg Model of the
970 Neutral and Ionized Atmosphere (HAMMONIA) (Schmidt et al., 2006)).

971 Above the stratosphere, the low collision frequency means that CO₂ preferentially
972 radiates absorbed energy to space, resulting in a net cooling. Thus, the expected long-term
973 temperature trends in the mesosphere and lower thermosphere due to CO₂ are negative.
974 Ground based optical measurements of the Meinel emission bands of the hydroxyl (OH)
975 molecule produced by the exothermic hydrogen (H) – ozone (O₃) reaction ($H + O_3 \rightarrow OH^* + 3.34 \text{ eV}$)
976 + 3.34 eV) have been used extensively over almost six decades as a method of measuring
977 atmospheric temperature in the vicinity of the mesopause (Kvifte, 1961; Sivjee, 1992; Beig
978 et al. 2003; Beig 2006; Beig et al. 2008; Beig 2011). The emission is centred about 87 km
979 altitude and the rotational temperatures derived are representative of the kinetic
980 temperatures, weighted by the shape and width of the layer (~8 km full-width at half-
981 maximum (FWHM)). Temperatures thus obtained have always been considered ambiguous
982 to the extent that they are dependent on the altitude of the emitting layer, and they are
983 weighted by the altitude profile of that layer. In the case of the OH* layer, different
984 vibrational bands are known to be weighted towards different altitude layers (von Savigny
985 et al. 2012), and on short time scales, individual bands vary in altitude with diurnal, semi-
986 diurnal, annual, semi-annual and solar cycle variations (García-Comas et al., 2017; Liu and
987 Shepherd, 2006; Mulligan et al., 2009). Over long timescales (more than one solar cycle)
988 however, recent studies using satellite data (Gao et al., 2016; von Savigny, 2015) and OH
989 Chemistry-Dynamics (OHCD) models have shown that, the OH* layer altitude is
990 remarkably insensitive to changes in CO₂ concentration or solar cycle variation. This
991 makes these measurements very valuable for monitoring long term changes in the
992 atmosphere.

993 This work provides an update on the solar cycle and long term trend analysis of the
994 OH rotational temperature measurements taken through each winter season at Davis
995 Research Station, Antarctica ([68° S, 78° E](#)). The dataset used here extends for 24
996 consecutive years and this analysis includes a further 8 years of measurements since the
997 previously published trend assessment using these data (French and Klekociuk, 2011).
998 Here we expand on the earlier analysis to provide a more detailed assessment of the solar
999 response, trends and variability in the Davis record in comparison with v4.2 measurements
1000 from the Microwave Limb Sounder (MLS) on the Aura satellite (Aura/MLS) and a network
1001 of similar ground based observations (coordinated by the Network for Detection of
1002 Mesospheric Change; (NDMC), Reisin et al. 2014).

1003 The outline of this paper is as follows. The instrumentation used and the acquired
1004 rotational temperature data collection are presented in Sections 2 and 3. Analysis of solar
1005 cycle response and the long-term linear trend is undertaken in Section 4 including
1006 comparisons with other ground-based observers and satellite measurements. Discussion of
1007 the results, summary and conclusions drawn are given in Sections 5 and 6, respectively.

1008 We use the following terminology for the analysed temperature series in this manuscript.
1009 From the measured temperatures and their nightly, monthly, seasonal or winter means,
1010 *temperature anomalies* are produced by subtracting the climatological mean or monthly
1011 mean (we fit solar cycle and linear trend to the anomalies), *residual temperatures*
1012 additionally have the solar cycle component subtracted (used in discussion of long-term
1013 trends) and *detrended temperatures* additionally have the long term linear trend subtracted
1014 (used in discussion about remaining variability).

1015

1016 **2. Instrumentation**

1017 A SPEX Industries Czerny-Turner grating spectrometer of 1.26 m focal length has
1018 been used to autonomously scan the OH(6-2) P-branch emission spectra (λ 839-851 nm) at
1019 Davis (68.6° S, 78.0° E) each winter season over the last 24 years (1995-2018). Night-time
1020 observations (sun $> 8^\circ$ below the horizon) are only possible between mid-February (~day
1021 048) and end of October (~day 300) at [the latitude of](#) Davis.

1022 The spectrometer views the sky in the zenith with a 5.3° field-of-view and an
1023 instrument resolution of ~ 0.16 nm, sufficient to separate P_1 and P_2 branch lines but not to
1024 resolve their Lambda-doubling components. Observations are made regardless of cloud or
1025 moon conditions and take of the order of 7 minutes to acquire a complete spectrum.

1026 Spectral response calibration has been maintained by reference to several tungsten filament
1027 Low Brightness Source units (a total of 4164 scans over the 24 years at Davis) which are
1028 in turn cross referenced to national standard lamps at the Australian National Measurement
1029 Institute (a total of 781 cross reference calibrations over 24 years). The response correction
1030 accounts mainly for the fall-off in response of the cooled gallium arsenide (GaAs)
1031 photomultiplier detector and amounts to 8.5% between the $P_1(2)$ and $P_1(5)$ of the OH(6-2)
1032 band. The total change in spectral response correction over 24 years is less than 0.3%
1033 (equates to less than 0.3 K for the $P_1(2) / P_1(5)$ ratio) despite changing the diffraction grating
1034 in 2006 and four changes of the GaAs photomultiplier detector which are carefully
1035 characterised over the years. The assigned annual calibration uncertainty is generally < 0.3
1036 K except for 1995 (1.8 K) due to calibration via a secondary calibration lamp and in 2002
1037 (1.2 K) due to detector cooling problems. Further details of the instrument are contained in
1038 Greet et al. (1997) and French et al. (2000).

1039

1040 3. Davis 24 year rotational temperature dataset

1041 We use the three possible ratios from the $P_1(2)$, $P_1(4)$ and $P_1(5)$ emission line
1042 intensities to derive a weighted mean temperature. Intensity values are interpolated to a
1043 common time between consecutive spectra to reduce ~~errors-uncertainty~~ associated with the
1044 7 minute acquisition cycle time. The weighting factor is the statistical counting error (based
1045 on the error in estimating each line intensity, taken as the square-root of the total number
1046 of counts for each line). $P_1(2)$ is corrected for the ~2% contribution by $Q_1(5)$, computed
1047 using the final weighted temperature. Line backgrounds are selected to balance the small
1048 auroral contribution of the N_2 1PG and N_2^+ Meinel bands and solar Fraunhofer absorption
1049 for spectra acquired under moonlit conditions. Correction factors account for the
1050 difference in Lambda-doubling between the P-branch lines determined with knowledge of
1051 the instrument line shape from high-resolution scans of a frequency-stabilized laser.

1052 Langhoff et al. (1986) transition probabilities are used to derive rotational
1053 temperatures as they are closest to the experimentally measured, temperature independent
1054 line ratios determined for the OH(6-2) band using the same instrument in French et al.,
1055 2000. Recent work by ~~(Noll S., Winkler, H., Goussev, O., and Proxauf et al.; (2020) Noll et~~
1056 at (2020), show that these remain a reasonable choice as the Langhoff et al (1986)
1057 coefficients show relatively small errors in the comparison of populations from P- and R-
1058 branch lines, as well as those of van der Loo and Groenenboom (2008) and Brooke et al.
1059 (2016). (see French et al., 2000).—Other published sets (e.g., Mies, 1974; Turnbull and
1060 Lowe, 1989; van der Loo and Groenenboom, 2007; Brooke et al., 2016) can ~~change-offset~~
1061 the absolute temperatures derived by up to 12 K. While the choice is important for
1062 comparisons of absolute temperature between observers, it does ~~, but does not~~
1063 significantly ~~not~~ affect the trend analysis reported here (as long as the same transition
1064 probability set has been used consistently for all years) ~~here~~ as the offset is removed by

Formatted: Subscript

Field Code Changed

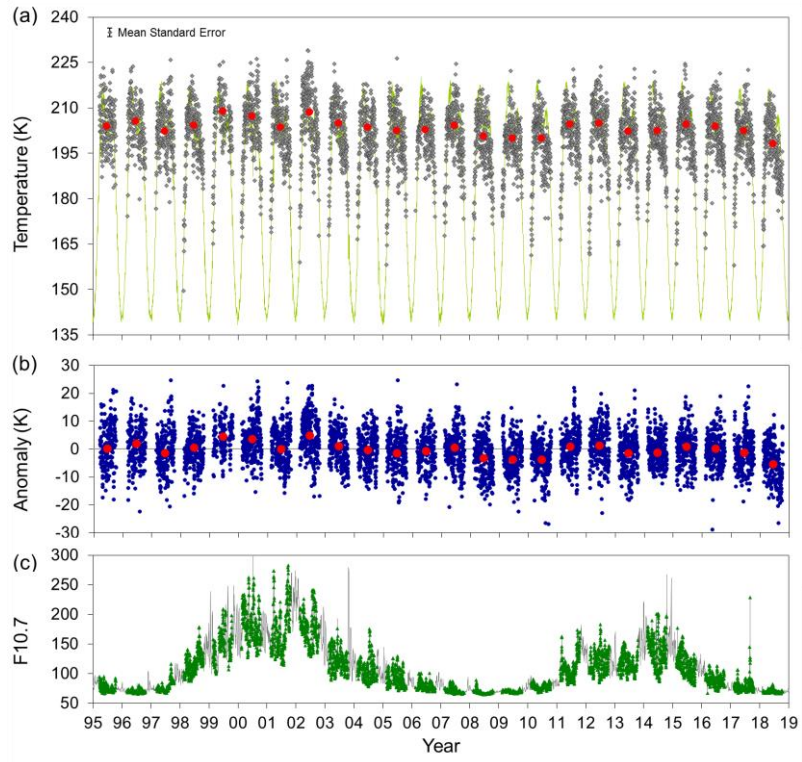
1065 ~~subtracting the climatological mean (trends are derived from temperature *anomalies*). It~~
1066 ~~should be noted however that comparison of absolute temperatures with other observations~~
1067 ~~are significantly affected by different choices of transition probabilities.~~

Formatted: Font: Italic

1068 Selection criteria limit extreme values of weighted standard deviation (< 20 K) and
1069 counting error (< 15 K), slope (< 0.06 counts/Å), magnitude (< 250 counts per second) and
1070 rate of change (< 3 counts per minute) of the backgrounds and the rate of change of branch
1071 line intensities (< 6%) between consecutive scans.~~Selection criteria limit extreme values of~~
1072 ~~weighted standard deviation and counting error, slope and magnitude of the background~~
1073 ~~and the rate of change of branch line intensities between consecutive scans.~~ Further details
1074 of the rotational temperature analysis procedure are available in Burns et al. (2003) and
1075 French and Burns (2004).

1076 Of over 624,000 measurements (typically ~26,000 profiles/year), 403,437 derived
1077 temperatures pass the reasonably tight selection criteria (many low signal-to-noise ratio
1078 profiles taken through thick cloud or high background profiles around full moon are
1079 rejected). These yield 5,309 nightly mean temperatures, where there are at least 10 valid
1080 samples that contribute within ±12 hours of local midnight (~1850 Universal Time (UT)).
1081 The time series spans two solar cycles (cycles 23 and 24) with peaks in 2001 and 2014.
1082 Annual mean temperatures show a dependence on solar activity (see French and Klekociuk
1083 (2011) for a comparison of different measures of solar activity with the Davis OH
1084 temperature data). We use the 10.7-cm solar radio flux index (F10.7; 1 solar flux unit (sfu)
1085 = $10^{-22} \text{ W m}^{-2} \text{ Hz}^{-1}$) as our preferred measure of solar activity (F10.7 is fitted and subtracted
1086 to examine residual variability). A plot of the nightly and winter mean temperatures with
1087 the F10.7 time series used in this work is provided in Fig. 1.

1088



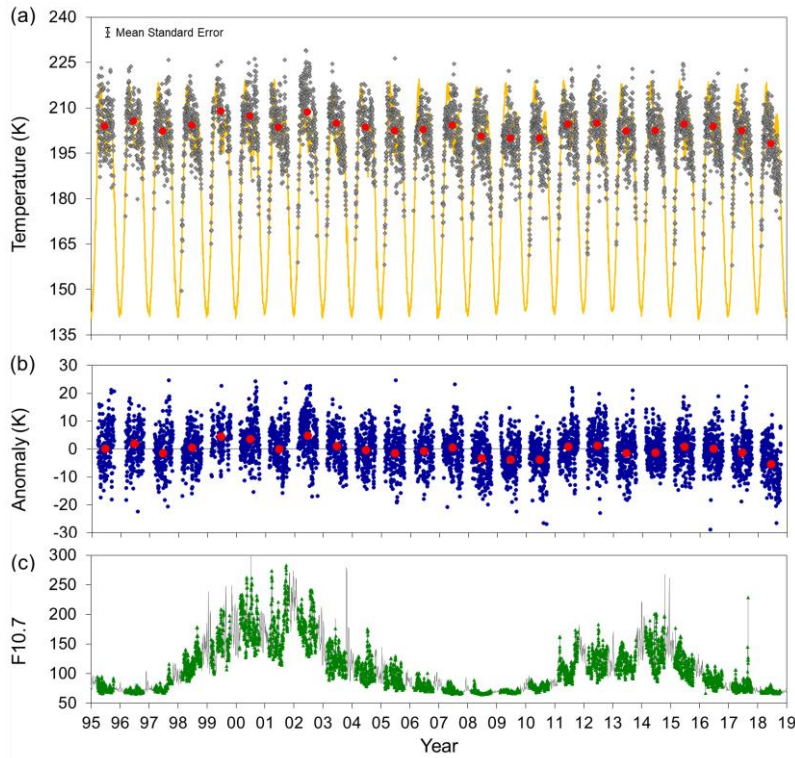
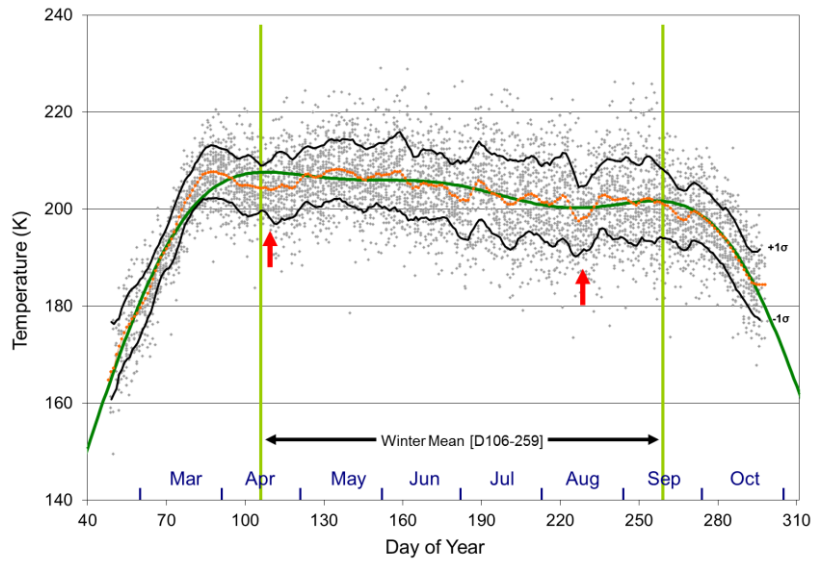


Figure 1 (a). Davis nightly mean temperatures (grey dots; 5309 samples) and winter mean temperatures (D106-259; red points) plotted over the [MSISE90-NRL-MSISE00](#) model temperature for 68°S (87 km altitude, local midnight values) for seasonal reference ([Picone et al., 2002](#); [Hedin, 1991](#); [Picone et al., 2002](#); gold line). (b). nightly mean and winter mean temperature anomalies derived by subtracting the climatological mean (see text) and (c). Daily mean F10.7 cm solar flux index (green points correspond to Davis OH temperature samples [over the grey line which are all daily observations](#))

A climatological mean is derived from a fit to the superposition of nightly mean temperatures for all annual series ([Fig. 2](#)). The climatological mean is characterised by a rapid autumn transition (February-March) increasing at 1.2 K/day until a turn-over about 29 March (day of year D088), a slow winter decline (April-September) of -0.4 K/day that is punctuated by mid-April (~D113) and mid-August (~D227) dips corresponding to reversals in the mean meridional flow ([Murphy et al., 2007](#)), followed by a rapid spring transition (October-November) of -1.0 K/day. [Figure 2 shows the superposed nightly](#)

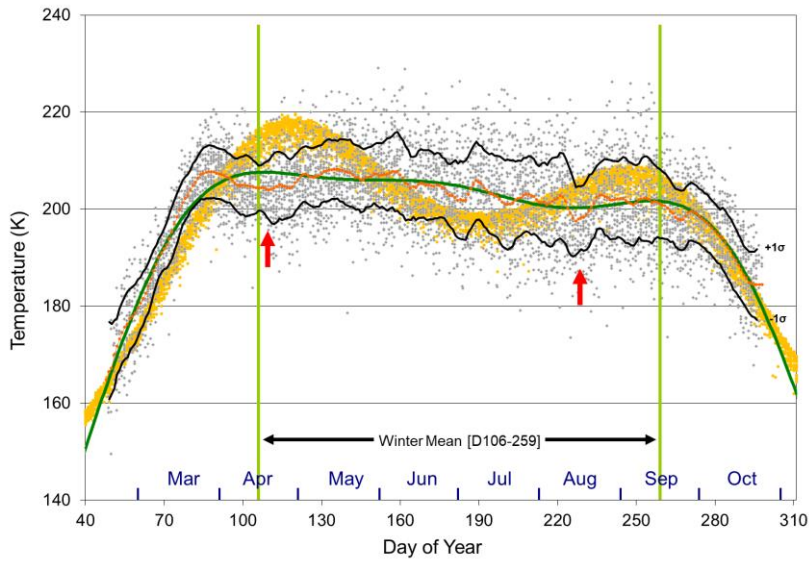
1107 ~~means for each year and the climatological mean fit~~ Subtracting the climatological mean
1108 produces 5309 nightly mean temperature anomalies. Winter mean temperatures are
1109 calculated over the interval from 15 April (D106) to 15 September (D259) which avoids
1110 the winter to summer transition intervals and lower numbers of nightly observations due to
1111 the shorter night length in March and October. A seasonal fit (annual amplitude 41.9 K,
1112 semi-annual 23.0 K, ter-annual 7.5 K; green line) and the NRL-MSISE00 reference
1113 atmosphere (87 km altitude, local midnight values for Davis; gold points) are also added
1114 to Fig. 2 for reference and comparison. The model is limited in its representation of the
1115 seasonal cycle as only annual and semi-annual terms are modeled.

1116



1117

Formatted: Left



1|18

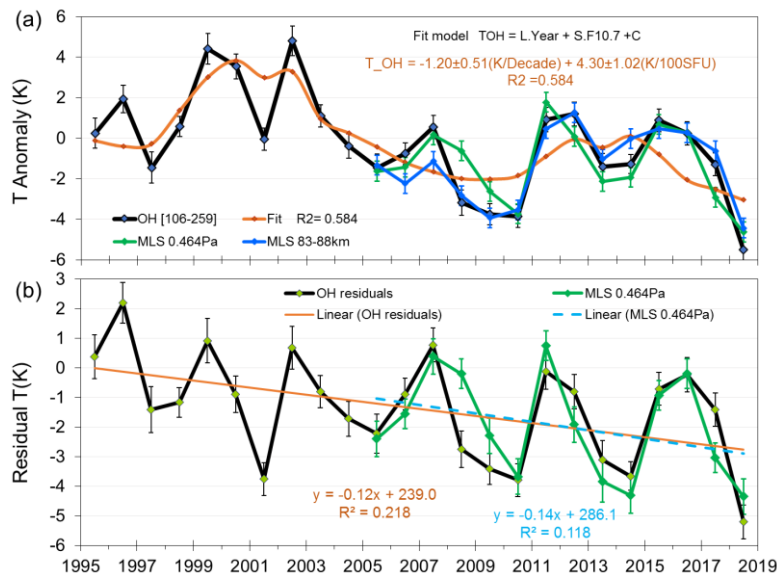
1|19 Figure 2. Superposed nightly mean temperatures from 1995 to 2018 [graygrey
 1|20 points] and a 5-day running mean which represents the climatological mean [orange line]
 1|21 with 1σ intervals [black lines]. The seasonal variation [green–annual, semi-annual, ter-
 1|22 annual fit; green line] is characterised by a rapid autumn transition (Feb–Mar) increasing at
 1|23 1.2 K/day until a turn over about 29th March (day 088), a slow winter decline (Apr–Sep) of
 1|24 -0.4 K/day, punctuated by mid-April and mid-August dips [indicated by red arrows]
 1|25 are also indicated, followed by a rapid spring transition (Oct–Nov) of 1.0 K/day. Green
 1|26 vertical lines mark the calculation region for winter mean temperatures (outside-avoiding
 1|27 spring and autumn the winter to summer transition intervals). The NRL-MSISE00 reference
 1|28 atmosphere (local midnight values for Davis) is also added for comparison [gold points]
 1|29

1130 4. Trend Assessment

1131 4.1 Davis winter mean trends

1132 Winter mean temperature anomalies over the 24 years of observations are plotted
1133 in Fig. 3a. The time series is fitted with a linear model containing a solar cycle term (F10.7)
1134 and long term linear trend. This model yields a solar cycle response coefficient (S) of 4.30
1135 ± 1.02 K/100sfu (95% confidence limits 2.2 K/100sfu $< S < 6.4$ K/100sfu) and a long term
1136 linear trend (L) of -1.20 ± 0.51 K/decade (95% confidence limits -0.14 K/decade $< L < -$
1137 2.26 K/decade) and accounts for 58% of the temperature variability.

Formatted: Font: Italic
Formatted: Font: Italic
Formatted: Font: Italic
Formatted: Font: Italic



1138
1139 Figure 3 (a). Winter mean (D106-259) temperature anomalies (black line) for Davis
1140 station (68°S, 78°E) fitted with a linear model containing a solar cycle term (F10.7cm flux)
1141 and long term linear trend (orange line). Fit coefficients are 4.30 ± 1.02 K/100sfu (95%
1142 confidence limits 2.18 to 6.42 K/100sfu) and -1.20 ± 0.51 K/decade (95% confidence limits
1143 -0.14 to -2.26 K/decade) respectively and account for 58% of the temperature variability.
1144 Also plotted (from 2005) are Aura/MLS temperature anomalies derived from the AMJJAS
1145 means of all satellite observations within 500 km of Davis station. (b) As for (a), but with
1146 the solar cycle component removed to better reveal the long term trend and quasi-
1147 quadrennial oscillation (QOO). OH residuals (black line) are compared with Aura/MLS
1148 temperature residuals at the 0.00464 hPa level, corrected with the same solar cycle
1149 component as used for the Davis OH measurements.

1150 [The stability of trend coefficients were tested for the presence of sampling gaps in](#)
1151 [the OH temperature record. With the exception of 1999 when 2 intervals D095-126 and](#)
1152 [213-249 were used to scan the OH\(8-3\) band and 1996 missing D176-202 all other years](#)
1153 [only have more than 85% nights within the winter averaging window sampled. \(ie 85% of](#)
1154 [the nights have a valid nightly average temperature with at least 10 measurements that pass](#)
1155 [selection criteria\). A sample bias could be introduced in computing the anomalies if there](#)
1156 [was a significant departure from the climatological mean in those intervals. The test](#)
1157 [examined the effect on the derived coefficients by omitting individual years sequentially](#)
1158 [from the model fit computation. These show the range of \$L\$ and \$S\$ coefficients if a data gap](#)
1159 [for the entire winter interval was missing in a particular year. All coefficients derived from](#)
1160 [the omitted year computations remained within the uncertainty limits of the solar cycle and](#)
1161 [long-term trend coefficients when all years were included.](#)

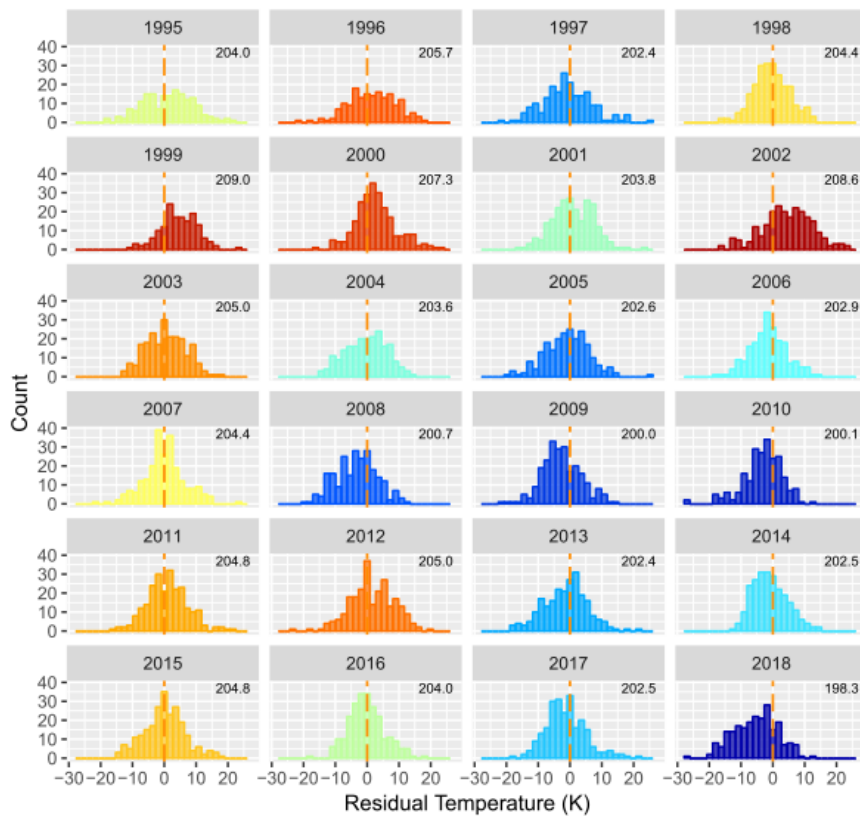
1162 We ~~note-report~~ that a new record low winter-mean temperature [of 198.3 K](#) was set
1163 for the Davis measurements in 2018, ~~with a value of 198.3 K,~~ which is 1.7 K below the
1164 previous minimum recorded in 2009 (200.0 K). This is not entirely due to the low solar
1165 activity in 2018 (winter mean flux of 70.4 sfu) as both 2008 (66.9 sfu) and 2009 (69.1 sfu)
1166 had lower mean flux and comparable years 1996 (70.6 sfu) was 7.4 K warmer (205.7 K)
1167 and 2007 (71.9 sfu) was 6.1 K warmer (204.4 K).

1168 Extracting the solar cycle contribution from the time series yields the long term
1169 linear trend and residual variability plotted in Fig. 3b. It is apparent from this plot that a
1170 significant oscillation on an approximately 4-year (quasi-quadrennial) timescale remains.
1171 A least-squares fit of a sinusoidal function to the data yields a period of 4.2 years and peak-
1172 peak amplitude of ~3 K. This feature will be examined in detail in Part 2 of this work
1173 (French, [W. J. R., Klekociuk, A. R., Mulligan et al., 20192020](#)).

Formatted: Font: Italic

Formatted: Font: Italic

1174 Distributions of the nightly mean residual temperatures for each year are shown for
 1175 comparison in Fig. 4. Histogram colour scale indicates the winter mean temperature from
 1176 warmest year (1999; red) to coldest year (2018; blue). Distributions vary between years
 1177 from sharp normal distributions (e.g., 1998, 2007, 2016), to broad flat distributions (e.g.,
 1178 1996, 1997), to skewed or double peaked distributions (e.g., 2004, 2012, 2014, 2018).
 1179 These differences can be attributed to the variability in large scale planetary wave activity
 1180 from year to year (French and Klekociuk, 2011)



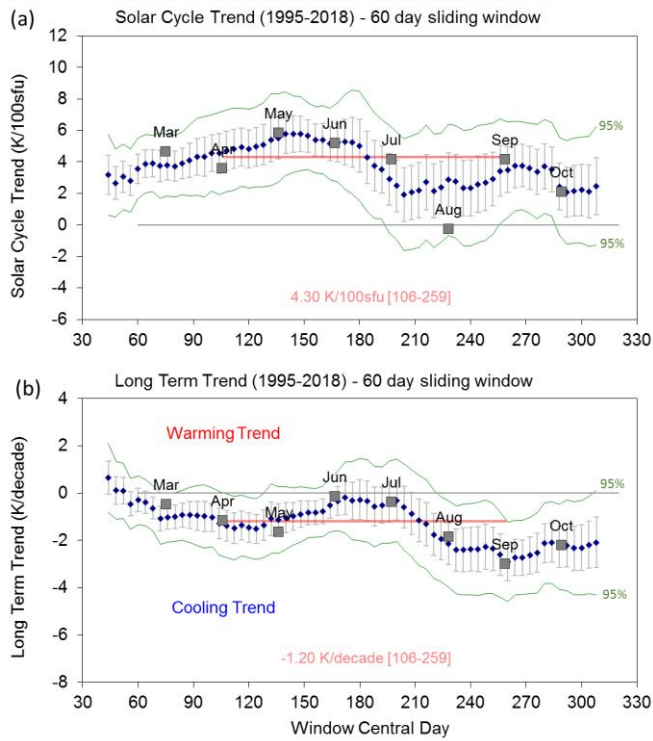
1181
 1182 Figure 4. Histograms of nightly mean residual temperatures showing the
 1183 distribution about the mean winter temperature (annotated in top right corner) coloured
 1184 from red (warmest year: 1999) to blue (coldest year: 2018).
 1185

1186 4.2 Seasonal variability in trends.

1187 Seasonal trend coefficients are ~~also somewhat variable~~[examined using a 60 day](#)
1188 [sliding window, and also from monthly average anomalies](#). Figure 5 shows the seasonal
1189 variability in solar cycle and long-term trend coefficients ~~derived using a 60 day sliding~~
1190 ~~window, and as monthly trends as~~ compared to the winter mean trends ([D106-259, 154 day](#)
1191 [mean](#); red lines) derived for Fig. 3. Seasonal solar response shows a maximum in May-
1192 June (~5 K/100sfu) and minimum around August (~2 K/100sfu). Note that April and
1193 August temperatures are affected by the characteristic dips seen in the climatological mean
1194 during these months (see Fig. 2). Linear trend coefficients show maximum cooling
1195 responses in April-May (~ -1.3 K/decade) and in August-October (~ -2.5 K/decade).
1196 Virtually no long-term cooling trend is apparent for the midwinter months of June-July.

1197

1198



1199

1200 Figure 5. The seasonal variability in (a) solar cycle and (b) long-term trend
 1201 coefficients derived using a 60 day sliding window (blue dots), and as monthly trends (grey
 1202 boxes) compared to the winter mean trends (red lines) derived for Fig. 3. The green lines
 1203 show the confidence limits (95%) for the trend coefficients.

1204

1205 4.3 Aura/MLS trend comparison

1206 For comparison with the Davis trend measurements, we use version v4.2 level 2
 1207 data from the Microwave Limb Sounder (MLS) instrument on the Earth Observing System
 1208 Aura satellite launched in July 2004 (Schwartz et al., 2008). Aura/MLS provides almost
 1209 complete global coverage (82° S-82° N) of limb scanned vertical profiles (~5-100 km) of
 1210 temperature and geopotential height derived from the thermal microwave emissions near
 1211 the spectral lines 118 GHz O₂ and 234 GHz O¹⁸O. Previous comparisons of these data
 1212 with MLS v2.2 temperatures were conducted by French and Mulligan, 2010.

1213 Over-plotted in Fig. 3a (extending from 2005) are the equivalent Aura/MLS mean
1214 temperature anomalies computed by averaging all observations within 500 km of Davis,
1215 for months April to September (AMJJAS) over altitudes 83-88 km (blue line, obtained
1216 from a linear interpolation of Aura/MLS geopotential height profiles to geometric height
1217 in 1 km steps) and at the 0.00464 hPa (native Aura/MLS retrieval) pressure level (green
1218 line). The Aura/MLS data were selected according to the quality control recommendations
1219 described in (Livesey, Nathaniel J., William G. Read, Paul A. Wagner, Lucien Froidevaux
1220 et al., (2018) Livesey et al. (2018). Approximately 60 samples per month (~2 per day) are
1221 coincident within this range. We see very close agreement to both the pressure and
1222 interpolated altitude coordinates considering that at these altitudes the vertical resolution
1223 (FWHM of the averaging kernel) of Aura/MLS is approximately 15 km (Schwartz et al.,
1224 2008), compared to the ~8km FWHM integration of the hydroxyl layer temperatures. The
1225 Aura/MLS measurements closely follow the solar response, the long-term linear trend and
1226 the magnitude and period of the quasi-quadrennial oscillation (QO) and the underlying
1227 long-term linear trend.

1228 We prefer the use of Aura/MLS pressure level data for the comparison with OH
1229 temperatures since it is the concentration (density) of reacting species that governs the
1230 hydroxyl layer position (primarily collisional quenching with O₂ and N₂ on the bottom-side
1231 of the layer, and reaction with atomic oxygen on the top-side of the layer; eg Xu et al.,
1232 2012). Statistically, (-from a chi-squared fit to the anomalies) the closest agreement is with
1233 the 0.00464 hPa pressure level and this is over-plotted on Fig. 3b corrected for using the
1234 same solar cycle response that was determined from the Davis OH measurements. The
1235 linear long-term trend fit for Aura/MLS over 14 years is -1.43 ± 1.1 K/decade which
1236 compares very well (comparable to the -1.2 ± 0.51 K/decade for the 24 years of Davis OH
1237 measurements, considering the seasonal variability shown above (section 4.2) and the) but

Formatted: Subscript

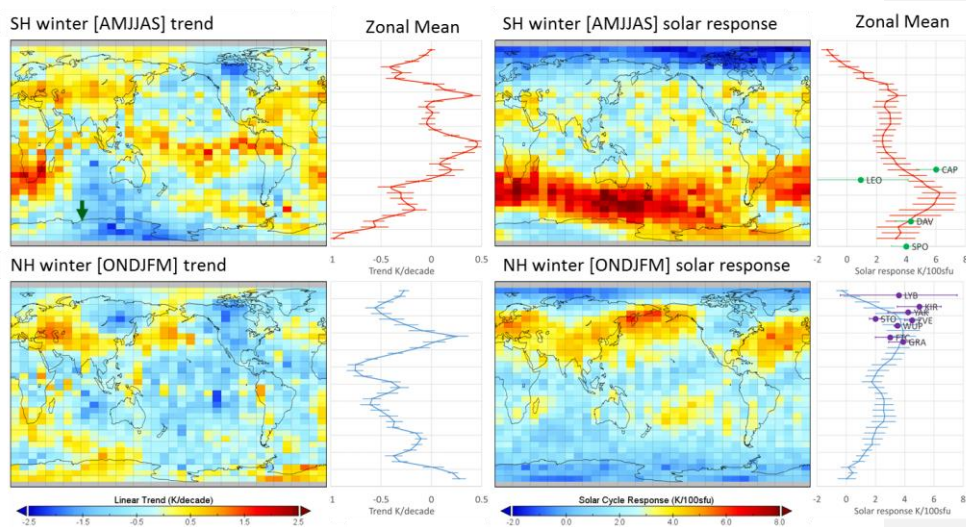
Formatted: Subscript

1238 ~~clearly the underlying QOO variability~~ residual evident in both series, which has a
1239 ~~significant effect on the fit over the different data spans~~ ~~has a significant effect on the fit.~~

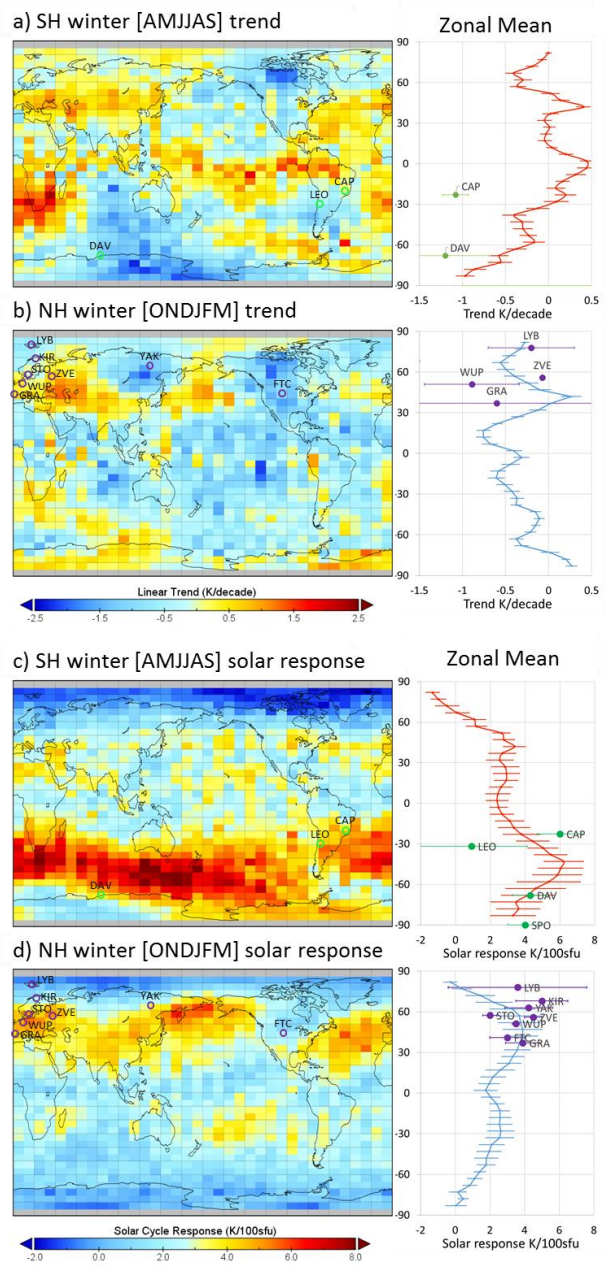
1240 It is important to note that the winter mean residual trend coefficients in Fig. 3b are
1241 ~~derived as a mean across 6 months of significantly varying solar and long term responses.~~
1242 ~~Nevertheless, the residual QOO signature remains readily apparent in the 60 day sliding~~
1243 ~~window means through April to July [AMJJ] although somewhat breaking down in August~~
1244 ~~to October [ASO].~~

1245 We examine the QOO feature in ~~more~~ greater detail in the second part of this work
1246 (French, ~~W. J. R., Klekociuk, A. R., Mulligan et al., 2019~~ 2020), but here, given the close
1247 agreement of Davis and Aura/MLS 0.00464 hPa trends in Fig. 3b, we apply the same model
1248 fit procedure to derive Aura/MLS solar cycle and linear long-term trend coefficients to
1249 obtain a global picture of trends at the hydroxyl layer equivalent pressure level (0.00464
1250 hPa). Figure 6 shows global trends determined by averaging Aura/MLS pressure level
1251 0.00464 hPa temperature anomalies into a $5^\circ \times 10^\circ$ (latitude x longitude) grid, over
1252 Southern Hemisphere (SH) winter months (April-September: AMJJAS; panel a) trend;
1253 panel c) solar response; top panels) compared to Northern Hemisphere (NH) winter months
1254 (October-March; ONDJFM; panel b) trend; panel d) solar response; bottom panels). Each
1255 grid box has been corrected for the solar cycle response determined from a linear regression
1256 of temperature to F10.7 over the 14 years of Aura/MLS measurements. The long-term
1257 linear trend (~~left hand panels~~ panels a) and b) and solar cycle response (~~right hand~~
1258 ~~panels~~ panels c) and d)), for each grid box, together with their corresponding zonal means
1259 are presented. The maps contain some interesting features; enhanced bands of solar activity
1260 response occur at mid-latitudes in both winter hemispheres although strongest in the SH
1261 (colour scales are the same for each hemisphere). Minima in sensitivity to solar forcing
1262 occur over the equator and the poles. Long-term trends over the Aura/MLS era are not

1263 globally uniform. While the global mean trend for the SH winter [AMJJAS] is -0.31
 1264 K/decade, there are regions of warming, notably around the equator, southern Africa,
 1265 Europe and the Atlantic ocean and strongest cooling over Antarctica and northern Canada.
 1266 For the NH winter [ONDJFM] the global mean is -0.11 K/decade with generally global
 1267 cooling, except for warming over Antarctica, Europe, southern Africa and the northern
 1268 Pacific Ocean.



1269
 1270
 1271



1272

1273 Figure 6. Global temperature trends (a. & b.) and solar cycle responses (c. & d.), together
 1274 with their corresponding zonal means determined from 14 years of MLS v4.2 pressure
 1275 level 0.0046hPa (hydroxyl layer equivalent), averaged into 5° latitude x 10° longitude grid,

1276 and over southern hemisphere winter months (AMJJAS; ~~top panels a. & c.~~) compared to
1277 northern hemisphere winter months (ONDJFM; ~~bottom panels b & d.~~) The linear trend and
1278 solar cycle response coefficients have been derived individually for each grid box from
1279 Aura/MLS over 14 years with no lag. ~~The green arrow in panel 1~~Station locations indicates
1280 the Aura/MLS comparison with ~~Davis shown in Fig 1B~~ground based observations of long-
1281 ~~term trend and solar response given in Table 1. Solar response coefficients from other~~
1282 ~~observers are indicated on the zonal solar response plots (see text for site information)~~
1283

1284

1285 4.4 Trend comparisons with other ground based observations

1286 It is useful to compare these Aura/MLS derived solar response and trend
1287 coefficients with other observations, carefully bearing in mind that these observations may
1288 span different time intervals than available in the Aura/MLS measurement epoch. At Davis
1289 the solar cycle response (indicated by the green ~~dot-point and label~~ DAV in Fig. 6 c.)
1290 determined over 24 years matches well with the zonal mean at 68° S determined from the
1291 Aura/MLS measurements. Davis appears to be on the poleward boundary of the strong
1292 band of solar sensitivity (~40-70° S) in the SH winter. The long-term trend at Davis is
1293 marked by the green ~~arrow-point and label~~ DAV on ~~the left hand upper~~ panel a) in Fig 6,
1294 and as we have seen from Fig. 3, agrees well with Aura/MLS.

1295 Table 1 summarises the data-span, derived long term trend, and solar cycle
1296 coefficients from a collection of ground-based observers. ~~Where new results are available~~
1297 ~~these have been updated from Table 2 in French and Klekociuk (2011) and as compiled in~~
1298 ~~Beig et al. (2008). Solar cycle and long-term trend coefficients from these sites are also~~
1299 ~~marked on Fig 6 where possible.~~ The majority of these observations agree well (within
1300 error estimates) with the Aura/MLS zonal mean solar response and long term trends
1301 evaluated here, given the different measurement epochs and geographic variability in the
1302 trends coefficients shown by Aura/MLS.

1303 ~~it is a zonal mean response.~~

1304

Site	Data Span	Trend K/decade	Solar response K/100sfu	Reference
Longyearbyen (LYB, 78°N, 16°E)	1983-2013	-0.2±0.5	3.6±4.0	Holmen et al. (2014)
Kiruna (KIR, 68°N, 21°E)	2003-2014	-2.6±1.5	5.0 ± 1.5	Kim et al. (2017)
Yakutia (YAK, 63°N, 129°E)	1999-2013	Not Significant	4.24±1.39	Ammosov et al. (2014)
Stockholm (STO, 57°N, 12°E)	1991, 1993-1998	Not Determined	2.0±0.4	Espy et al. (2011)
Zvenigorod (ZVE, 56°N, 37°E)	2000-2016	-0.07±0.03	4.5±0.5	Perminov et al. (2018)
Wuppertal (WUP, 51°N, 7°E)	1988-2015	-0.89±0.55	3.5±0.21	Kalicinsky et al. (2016)
Fort Collins (FTC, 41°N, 105°W)	1990-2018	-2.3±0.5	3.0±1.0	Yuan et al. (2019 in press)
Granada (GRA, 37°N, 3°W)	2002-2015	-0.6±2.0	3.9±0.1	Garcia-Comas et al. (2017)
Cachoeira Paulista (CAP, 23°S, 45°W)	1987-2000	-1.08±0.15	6±1.3	Clemesha et al. (2005)
El Leoncito (LEO, 32°S, 69°W)	1998-2002	Not Determined	0.92±3.2	Scheer et al. (2005)
Davis (DAV, 68°S, 78°E)	1995-2018	-1.20±0.51	4.30±1.02	This Work
South Pole (SPO, 90°S)	1994-2004	0.1±0.2	4.0±1.0	Azeem et al. (2007)

1305 Table 1. A comparison of solar cycle response and temperature trend observations from
1306 the ground-based OH observer network with updates since 2011 where available.
1307
1308
1309

1310 As some observers have found, there is a [significantimportant](#) question about a time
1311 delay in the OH layer temperature response to solar forcing via the various solar absorption
1312 mechanisms in the atmosphere. The major absorbers and altitude of solar extreme
1313 ultraviolet radiation are molecular oxygen (Schumann-Runge continuum, 80-130 km,
1314 Schumann-Runge electronic and vibrational bands, 40-95 km, Herzberg continuum, below
1315 50 km) and ozone (Hartley-Huggins bands, below 50 km).

1316 We have previously found a lag of around 160 days (F10.7 leads temperature) is
1317 best fit to the linear model (French and Klekociuk, 2011), others find shorter: 80 days at
1318 Longyearbyen, Svalbard (Holmen et al. 2014), or larger lags: 25 months at Maimaga station,
1319 Yakutia (Ammosov et al. 2014; Reisin et al. 2014). Recalculating the long term trends for
1320 Aura/MLS assuming a uniform global solar response (as for Davis), or with a 160 day lag
1321 and zonal mean solar response ([see supplementary material](#)) does not significantly change
1322 the warming and cooling patterns shown in Fig. 2, but the lag does reduce the cooling trend

1323 (on average by 0.16 K/decade for the southern hemisphere ~~(SH)~~-winter and 0.11 K/decade
1324 for the northern hemisphere ~~(NH)~~ winter) and increases the fit error.

1325 Beig (2011a, 2011b) in their reviews of long-term trends in the temperature of the
1326 mesosphere and lower thermosphere (MLT), highlight the difficulty of distinguishing
1327 between the anthropogenic and solar cycle influences. In their results, mesopause region
1328 temperature trends were found to be either slightly negative or zero. At that time, it was
1329 believed that the solar response becomes stronger with increasing latitude in the
1330 mesosphere with typical values in the range of a few degrees per 100 solar flux units in the
1331 lower part of the mesosphere but reaching 4-5 K/100 sfu near the mesopause. More recent
1332 studies using longer data sets (Ammosov et al. 2014; Holmen et al. 2014; Perminov et al.
1333 2018) and satellite data (Tang et al. 2016) have reinforced that view.

1334 Trend breaks began to appear in mesopause region temperatures in 2006
1335 (Offermann et al., 2006, 2010), and these continue until now in certain locations (e.g.,
1336 Jacobi et al., 2015; Kalicinsky et al., 2018; Yuan et al., 2019). These can be quite varied
1337 from site to site, ranging from -10 K/decade to +5 K/decade. Some of these estimates
1338 simply suffer from lack of observations (measurement spans less than a solar cycle). Few
1339 are longer than 2 solar cycles, but those of note are included in Table 1. OH temperature
1340 trend studies in the southern hemisphere are less common. Reid et al. (2017) report MLT-
1341 region nightglow intensities, temperatures and emission heights near Adelaide (35° S, 138°
1342 E), Australia. Five years (2001-2006) of spectrometer measurements using OH(6-2) and
1343 O₂(0-1) temperature are compared with 2 years of Aura/MLS data and 4.5 years of SABER
1344 data. Venturini et al. (2018) report mesopause region temperature variability and its trend
1345 in southern Brazil (Santa Maria, 30° S, 54° W), based on SABER data over the period
1346 2003-2014. Nath and Sridharan (2014) examined the response of the middle atmosphere
1347 temperature to variations in solar cycle, QBO and ENSO in the altitude range 20-100 km

1348 and 10-15° N latitude using monthly averaged zonal mean SABER observations for the
1349 years 2002-2012. They found cooling trends in most of the stratosphere and the mesosphere
1350 (40–90 km). In the mesosphere, they found the temperature response to the solar cycle to
1351 be increasingly positive above 40 km. The temperature response to ENSO was found to
1352 be negative in the middle stratosphere and positive in the lower and upper stratosphere,
1353 whereas it appeared largely negative in the height range 60–80 km and positive above 80
1354 km.

1355

1356 5. Discussion

1357 5.1 Relationship between Davis trends and CO₂ ~~and O₃~~ change.

Formatted: Subscript

1358 Our updated trend assessment over 24 years yields a cooling rate of -1.20 ± 0.51
1359 K/decade for the mean winter [D106-259] temperatures in the hydroxyl layer above Davis.
1360 A slightly greater rate of -1.32 ± 0.45 K/decade is derived if the full year [D040-310] of
1361 observations are included in the annual means. Over the same period, annual mean surface
1362 CO₂ volume mixing ratios (VMRs) increased from 360.82 ppm [1995] to 408.52 ppm
1363 [2018] (Mauna Loa values from Global Greenhouse Gas Reference Network
1364 www.esrl.noaa.gov/gmd/ccgg/trends/), an increase of 47.7 ppm or 13.2% (19.9 ppm per
1365 decade or 5.5% per decade). Qian et al. (2019) quote a CO₂ trend figure of 5.2%/decade
1366 (or 5.1 % if the seasonal variation is removed before the linear trend calculated) based on
1367 measurements made by TIMED/SABER from 2002-2015. If the primary factor for the
1368 observed temperature trend is considered to be CO₂ radiative cooling, a coefficient of -0.06
1369 K/ppmCO₂ or -0.22 K/%CO₂ is implied. This is approximately twice the value obtained
1370 by (Huang, 2018) (her Figure 2) who employed a linear scaling of the result of a doubling
1371 of CO₂ concentration by (Roble and Dickinson, 1989). A CO₂ increase of 26.5% from
1372 1960 to 2015 was accompanied by a temperature decrease of 1.4% at an altitude of 89.4
1373 km near Salt Lake city, Utah (18° N, 290° E).

1374 CO₂ is well mixed through the lower atmosphere with a constant VMR up to about
1375 80 km. Above this height, diffusion and photolysis processes begin to have an effect,
1376 reducing the VMR (Garcia et al., 2014) but these processes vary with latitude and season
1377 (Rezac et al. 2015; López-Puertas et al., 2017).

1378 ~~Several studies of CO₂ VMR using profiles from the Atmosphere Chemistry~~
1379 ~~Experiment Fourier Transform Spectrometer (ACE-FTS) and Sounding of the Atmosphere~~
1380 ~~using Broadband Emission Radiometry (SABER) satellite instruments, reported~~

1381 considerably larger rates of change of CO₂ in the upper atmosphere, increasing from about
1382 5% per decade at 80 km to 12% per decade at 110 km (Emmert et al., 2012; Garcia et al.,
1383 2016; Yue et al., 2015). However, more recent analysis of the ACE-FTS and SABER CO₂
1384 data with different deseasonalizing procedures have shown an average rate of 5.5% per
1385 decade in the 80–110 km region, consistent with surface rates (Qian et al., 2019; Rezac et
1386 al., 2018).

1387 In a recent summary of progress in trends in the upper atmosphere. (Laštovička
1388 and Jan, (2017) Laštovička (2017) identified greenhouse gases, particularly CO₂ as the
1389 primary driver of long-term trends there. The overall effect of greenhouse gases at
1390 mesospheric altitudes is radiative cooling. The important secondary trend drivers in the
1391 mesosphere and lower thermosphere (MLT) are stratospheric ozone, water vapour
1392 concentration and atmospheric dynamics. Temperature trends are predominantly
1393 negative, and recent progress in understanding the magnitude of the cooling have arisen
1394 from confirmation and quantification of the role of ozone. Lübken et al. (2013) present
1395 the results of trend studies in the mesosphere in the period 1961–2009 from the Leibniz-
1396 Institute Middle Atmosphere (LIMA) chemistry-transport model which is driven with
1397 European Centre for Medium-Range Weather Forecasts (ECMWF) reanalysis below 40
1398 km, and observed variations of CO₂ and O₃. They find that CO₂ is the main driver of
1399 temperature change in the mesosphere, with O₃ contributing approximately one third to
1400 the trend. Linear temperature trends were found to vary substantially depending on the
1401 time period chosen primarily due to the influence of the complicated temporal variation
1402 of ozone. Figure 3 of (Lübken et al., 2013) show a monotonically increasing trend in
1403 CO₂ compared with a much more complicated temporal ozone variation (essentially
1404 constant until 1980, a rapid decrease from 1980–1995, followed by an increase since then.
1405 Trends in ozone vary as a function of both altitude and latitude, with positive trends

Formatted: Subscript

Formatted: Subscript

Formatted: Subscript

Formatted: Subscript

Formatted: Subscript

Formatted: Subscript

1406 [dominating in the lower stratosphere and mesosphere \(Laštovička, 2017\). Increases in](#)
1407 [water vapour concentration are considered a secondary but non-negligible effect](#)
1408 [particularly in the lower thermosphere \(Akmaev et al., 2006\)](#)~~(Akmaev et al., 2006)~~. [The](#)
1409 [trend effect of dynamics was found to be very slightly negative in the mesosphere, but](#)
1410 [very small compared with the radiatively induced trends. At the mesopause, the trend](#)
1411 [due to dynamics was positive and significantly larger \(~1 K/decade\). These results were](#)
1412 [found to be in good agreement with observations from lidars, Stratospheric Sounding](#)
1413 [Units \(SSU\) \(Randall et al., 2009\) and radio reflection heights which have decreased by](#)
1414 [more than 1 km in the last 50 years due to shrinking in the stratosphere/lower mesosphere](#)
1415 [caused by cooling](#)In a recent summary of progress in trends in the upper atmosphere,
1416 [Laštovička \(2017\) identified greenhouse gases, particularly CO₂ as the primary driver of](#)
1417 [long term trends there. The important secondary trend drivers in the mesosphere and](#)
1418 [lower thermosphere \(MLT\) are stratospheric ozone, water vapour concentration and](#)
1419 [atmospheric dynamics. The overall effect of greenhouse gases at mesospheric altitudes is](#)
1420 [radiative cooling. Temperature trends are predominantly negative, and recent progress in](#)
1421 [understanding the magnitude of the cooling have arisen from confirmation and](#)
1422 [quantification of the role of ozone. In the mesopause region, about two thirds of the](#)
1423 [cooling is attributed to increases in CO₂ concentration and one third to changing](#)
1424 [concentration of ozone in the stratosphere \(Lübken et al., 2013\). Increases in water](#)
1425 [vapour concentration are considered a secondary but non-negligible effect particularly in](#)
1426 [the lower thermosphere \(Akmaev et al., 2006\). Trends in ozone vary as a function of both](#)
1427 [altitude and latitude, with positive trends dominating in the lower stratosphere and](#)
1428 [mesosphere.](#)
1429 [Huang \(2018\) examined the influence of CO₂ increase, solar cycle variation and](#)
1430 [geomagnetic activity on airglow from 1960 to 2015 using two airglow chemistry](#)

1431 dynamics models (OHCD—OH chemistry dynamics, and MACD—multiple airglow
1432 chemistry dynamics). As expected, the results showed that airglow intensity and peak
1433 volume emission rate (VER) are in phase and have a linear relationship with F10.7
1434 values, whereas CO₂ increase leads to a slowly decreasing trend in OH(8-3) airglow
1435 intensity. OH(8-3) peak altitudes of the VER are unaffected by increases in CO₂
1436 concentration, and are only slightly affected by the F10.7 cycle, with slightly lower peak
1437 altitudes when F10.7 is <100 SFU. Surprisingly, OH VER peak heights showed a
1438 significant inverse relationship with geomagnetic activity as measured by the Ap index.
1439 We find no significant correlation of the *T* residual from Davis with the Ap index for the
1440 months of AMJJAS.

1441 ——— Lübben et al. (2013) present the results of trend studies in the mesosphere in the
1442 period 1961–2009 from the Leibniz Institute Middle Atmosphere (LIMA) chemistry-
1443 transport model which is driven with European Centre for Medium-Range Weather
1444 Forecasts (ECMWF) reanalysis below 40 km, and observed variations of CO₂ and O₃.
1445 They find that CO₂ is the main driver of temperature change in the mesosphere, with O₃
1446 contributing approximately one third to the trend. Linear temperature trends were found
1447 to vary substantially depending on the time period chosen primarily due to the influence
1448 of the complicated temporal variation of ozone. The trend effect of dynamics was found
1449 to be very slightly negative in the mesosphere, but very small compared with the
1450 radiatively induced trends. At the mesopause, the trend due to dynamics was positive and
1451 significantly larger (~1 K/decade). These results were found to be in good agreement
1452 with observations from lidars, Stratospheric Sounding Units (SSU) (Randall et al., 2009)
1453 and radio reflection heights which have decreased by more than 1 km in the last 50 years
1454 due to shrinking in the stratosphere/lower mesosphere caused by cooling. Figure 3 of
1455 (Lübben et al., 2013) show a monotonically increasing trend on CO₂ compared with a

1456 much more complicated temporal ozone variation (essentially constant until 1980, a rapid
1457 decrease from 1980–1995, followed by an increase since then.

1458 A recent paper by Hervig et al. (2019) report on the absence of a solar signal
1459 correlated response in polar mesospheric clouds (PMCs) in the summer mesopause
1460 following 2002. PMCs are controlled by temperature and water vapour. At solar maximum,
1461 temperatures are expected to be higher and water vapour lower, thereby leading to less
1462 PMCs at solar maximum. This anti-correlation was evident in satellite data until 2002, but
1463 has been absent since then. The main cause for the diminished solar cycle in PMCs at 68°
1464 N and 68° S appears to be the dramatic suppression of the solar cycle response in water
1465 vapour. The solar cycle response of temperature also decreases after 2002, but has a much
1466 lower effect on PMCs than the water vapour.

1467 ———The Whole Atmosphere Community Climate Model (WACCM) extended into
1468 thermosphere (upper boundary ~700 km) (WACCM-X) was used by Qian et al. (2019)
1469 (with the lower atmosphere constrained by reanalysis data) to investigate temperature
1470 trends and the effect of solar irradiance on temperature trends on the mesosphere during
1471 the period 1980-2014. The overall temperature trend in the mesopause region at 85 km
1472 was statistically insignificant at -0.46 ± 0.60 K/decade. Solar irradiance effects on the
1473 global average temperature are positive and decrease monotonically with decreasing
1474 altitude from a value of ~3 K/100 sfu in the lower thermosphere to ~1 K/100 SFU at 55
1475 km. This is readily explained by the decreasing external energy from the Sun with reducing
1476 altitude. A monthly mean global average trend of 2.46 K/100 sfu is quoted for the
1477 mesopause near 85 km. The mesosphere is affected by solar irradiance directly from local
1478 heating through absorption of radiation, and indirectly through dynamics by its effects on
1479 the geostrophic winds which control the upward propagation of gravity waves and
1480 planetary waves generated in the troposphere. Zonal mean temperatures show significant

1481 variability as a function of altitude, latitude and season. Qian et al. (2019) provide [globally](#)
1482 [zonal](#) averaged temperature trend values as a function of altitude ([50-110 km](#)) and latitude
1483 for each month ([their Fig. 3](#)) some of which are statistically significant. Solar cycle effects
1484 on temperature are in reasonable agreement with the [OH\(6-2\) temperaturesDavis](#)
1485 [coefficients](#) (shown in [Figure 5\(a\)](#)) with positive values ranging from ~3-5 K/100 sfu, the
1486 largest values occurring in July and October ([compare Qian et al. 2019 Fig 4.](#)). -The long-
1487 term trend is predominantly negative with values in the range -1 to -3 K/decade with the
1488 largest cooling occurring in March and September at the latitude and altitude of the OH
1489 temperatures measured at Davis Station. WACCM-X shows slightly positive trend values
1490 in the months of February, November and December at Davis Station, but OH(6-2)
1491 temperature data are not available in these months. The September maximum in cooling is
1492 in reasonable agreement with the Davis measurements shown in Figure 5 of this work.

1493 More recent results from Garcia et al. (2019) using WACCMv4 free-running
1494 (coupled ocean) simulations for the period 1955-2100 using IPCC RCP 6.0 attribute the
1495 changes in the trends of the temperature profile to monotonic increases in CO₂
1496 concentration together with a decrease in O₃ until 1995 followed by subsequent increase.
1497 Garcia et al. (2019) assign half of the stratopause negative temperature trend to ozone
1498 depleting substances. At the mesopause, the global mean trend in temperature is
1499 approximately -0.6 K/decade. Solar cycle signals at the mesopause are in the range 2-3
1500 K/100 sfu with slightly higher values in the southern polar cap. Very large seasonal trends
1501 in temperature at all altitudes are associated with the development of the Antarctic ozone
1502 hole. Trends are largest in the November-December period, and teleconnections are made
1503 with the upper mesosphere via GW filtering by the zonal wind anomaly in the southern
1504 polar cap.

1505

1506 5.2 Trend breaks.

1507 When analysing long-term trends, several authors (Lübken et al., 2013; Qian et al.,
1508 2019) emphasise the importance of specifying the length of the time period, as well as the
1509 beginning and end of the period, because trend drivers can be different for different periods
1510 (e.g., Yuan et al., 2019). Yuan et al. (2019) report long-term trends of the nocturnal
1511 mesopause temperature and altitude from LIDAR observations at mid-latitude (41-42° N,
1512 105-112° W) in the period 1990-2018. They divided their observations into two categories,
1513 the high mesopause (HM) above 97 km during the non-summer months, mainly formed by
1514 radiative cooling, and the low mesopause (LM) below 92 km during the non-winter months
1515 generated by mostly by adiabatic cooling. This idea of the mesopause at two different
1516 altitudes is well established (e.g., von Zahn et al., 1996; Xu et al., 2007; Thulasiraman and
1517 Nee, 2002). Although Yuan et al. (2019) obtained a cooling trend of more than 2 K/decade
1518 in the mesopause temperature along with a decreasing trend in mesopause height since
1519 1990, the temperature trend is statistically insignificant since 2000.

1520 Trend breaks have been reported at other mid-latitude stations (Offermann et al.,
1521 2006, 2010) where a discontinuity was found in the overall trend in the year 2001/2002.
1522 Using some of the same data as Offermann et al. (2006), Kalicinsky et al. (2016) reported
1523 a trend break in the middle of 2008. Before the break point, there is a clear negative trend
1524 reported to be -2.4 ± 0.7 K/decade, whereas after 2008, a large positive trend of 6.4 ± 3.3
1525 K/decade is ~~deciphered~~determined. Two possible explanations are suggested for the trend
1526 break: the first is that it is the result of a combination of the solar cycle and a long period
1527 oscillation such as the 22-year Hale cycle of the Sun. A second possible explanation of the
1528 very substantial change in the trend at 2008 is a combination of the solar flux with a
1529 sensitivity of 4.1 ± 0.8 K/100 SFU together with a long period oscillation 24-26 years with
1530 an amplitude of about 2K. Kalicinsky et al. (2018) find support for this idea in the

1531 identification of a quasi-decadal oscillation in the summer mesopause over Western Europe
1532 in plasma scale height observations (near 80 km altitude) which are in anti-correlation with
1533 the potential oscillation in temperature from OH* measurements. The anti-correlation in
1534 the two data sets is explained on the basis of the fact that they originate below (plasma
1535 scale height data) and above (OH* temperature data) the temperature minimum in the
1536 mesopause region in summer. Jacobi et al. (2015) find that the long-term behavior of both
1537 meridional and zonal winds at 90-95 km in northern mid-latitude stations exhibit trend
1538 breaks in summer near 1999, although the winter data are well described by a single linear
1539 trend over the years 1980- 2015. We find no obvious sign of a discontinuity in the trend
1540 obtained in the Davis data [from 1995-2018. There is no significant change in the long-](#)
1541 [term trend or solar response when extending the period of study from 16 years \(2005-2010](#)
1542 [coefficients \$4.79 \pm 1.02\$ K/100sfu and \$-1.18 \pm 0.87\$ K/decade; French and Klekociuk, 2011\)](#)
1543 [to 24 years \(this work\). Neither coefficient has changed outside the uncertainty.](#)

1544

1545 5.3 Effect of changes in the OH*-layer height

1546 There is widespread acceptance that cooling of the middle atmosphere due to
1547 increases in CO₂ concentration has resulted in shrinking of the middle atmosphere (e.g.,
1548 (Grygalashvyly et al., 2014; Sonnemann et al., 2015). This does raise the question
1549 however of whether the OH* layer is fixed to a constant pressure level rather than a
1550 constant altitude. There are mixed reports on this topic. In a long-term study of the
1551 effects of chemistry, greenhouse gases, and the solar modulation on OH* layer trends
1552 using the Leibniz Institute Middle Atmosphere (LIMA) chemistry-transport model
1553 covering the period 1969 to 2009, Grygalashvyly et al. (2014) reported a downward shift
1554 in the OH*-layer by about 0.3 km/decade in all seasons due to shrinking of the middle
1555 atmosphere resulting from radiative cooling by increasing CO₂ concentrations. Wüst et

1556 al. (2017) report a descent in the mean altitude of the OH* layer of 0.02 km/ year from 14
1557 years of SABER data (2002-2015) in the alpine region of southern Europe (44–48° N, 6–
1558 12° E). They refer to a paper by Bremer and Peters (2008) which reports low frequency
1559 reflection heights (ca. 80-83 km) between 1959 and 2006 and derive a figure of 0.032
1560 km/year.

1561 Sivakandan et al. (2016) have published a long-term variation paper on OH peak
1562 emission altitude and volume emission rate over Indian low latitudes using SABER data.
1563 A weak decreasing trend of 19.56 m/year was reported for the peak emission altitude of
1564 the night-time OH*-layer. ~~García-Comas et al. (2017)~~ [García-Comas et al. \(2017\)](#)
1565 [reported a slightly larger decrease of 40 m/decade in SABER OH volume emission rate](#)
1566 [weighted altitude at mid-latitudes which accompanied a 0.7%/decade increase in OH](#)
1567 [intensity and a 0.6K/decade decrease in OH equivalent temperature.](#)

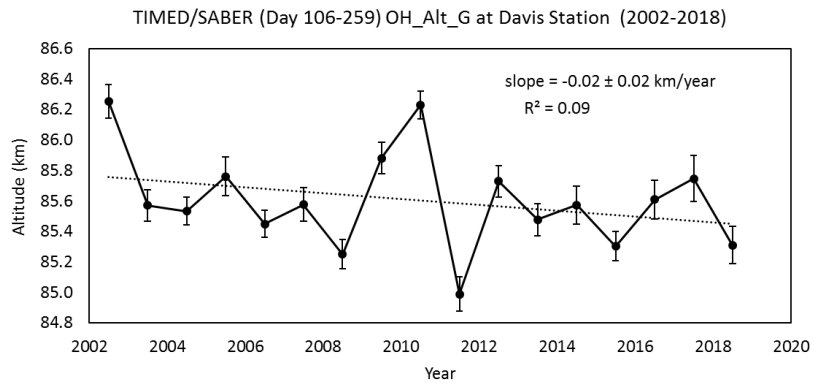
1568
1569 A vertical shift of the OH* layer either upward or downward gives rise to a change
1570 in the emission weighted temperature which is measured by ground-based optical
1571 instruments (French and Mulligan, 2010; Liu and Shepherd, 2006; von Savigny, 2015).
1572 Von Savigny (2015) reported no apparent trend or solar cycle in OH emission altitude at
1573 the local time of the SCIAMACHY nighttime observations in the period 2003-2011.
1574 However, Teiser and von Savigny (2017) found evidence of an 11-year solar cycle in the
1575 vertically integrated emission rate and in the centroid emission altitude of both the OH(3-
1576 1) and OH(6-2) bands in SCIAMACHY data. Gao et al. (2016) found no evidence that the
1577 OH* peak heights are affected by solar cycle in 13 years of TIMED/SABER data, and
1578 deduced that the solar cycle variation of temperature obtained from ground-based OH
1579 nightglow observations were essentially immune from the OH emission altitude variations.
1580 Huang (2018) found no systematic response of airglow O(¹S) green line, O₂(0-1), or OH(8-

Formatted: Line spacing: Double

1581 3) VER peak heights with the F10.7 solar cycle using two airglow models OHCD and
1582 MACD-90. The Huang (2018) result is supported by Gao et al. (2016) using
1583 TIMED/SABER data and by von Savigny (2015) using SCIAMACHY data. These
1584 confirmations of the remarkable long-term stability of the peak altitude of the OH*-layer
1585 in an atmosphere with increasing CO₂ concentration and changing solar radiation are
1586 essential for the use of long-term studies of mesopause region temperatures derived from
1587 ground-based OH* optical measurements.

1588 We have examined the altitude [variation](#) of the OH* layer [over Davis](#) during the
1589 period 2002-2018 using the OH-B channel volume mission rate (VER) from
1590 TIMED/SABER (version 2.0) sensitive in the wavelength range 1.56-1.72 μm, which
1591 includes mostly the OH(4-2) and OH(5-3) bands. All VER altitude profiles between day
1592 105 and day 259 that satisfied the selection criteria (tangent point within 500 km of Davis
1593 and solar zenith angle > 97°), employed by French and Mulligan (2010) were used to
1594 determine the altitude of the layer. The altitude of the peak was obtained from a
1595 Gaussian profile fitted to the VER profile (for more details, see French and Mulligan,
1596 2010). The slope of the best fit line to the winter annual average peak altitude was -0.02
1597 ± 0.02 km/ year as shown in Figure 7, i.e., no significant change in altitude of the layer
1598 over the period in agreement with the result of Gao et al. (2016).

1599



1600

1601 Figure 7. The trend in the mean winter OH layer altitude, derived from TIMED/SABER
 1602 (version 2.0) OH-B channel volume emission rate. The slope of the best fit line is $-0.02 \pm$
 1603 0.02 km/year, i.e., no significant change in altitude of the layer over this interval.

1604

1605 5.4 Global solar cycle and [linear-long-term](#) trends

1606 The [trend-long-term trend](#) measured at Davis is well matched with the result from
 1607 Aura/MLS over 14 years for the southern hemisphere (~~SH~~) winter months (AMJJAS) at
 1608 the 0.00464 hPa level. Clearly though, applying the same analysis to the global temperature
 1609 field reveals that trends are [far from](#) globally uniform (~~Fig 6~~) (~~Fig 6~~). In the SH winter
 1610 the most significant cooling trends are seen over the southern polar cap and northern
 1611 Canada, with warming trends over southern Africa, around the equator and over Europe
 1612 and Russia. NH winter cooling trends are strongest over eastern Russia and North America,
 1613 but warming trends remain over Europe.

1614 There are a number of limitations and assumptions made for these derived trends:
 1615 i) there are only 14 years from which to extract a solar cycle component, ii) a solar cycle
 1616 component is computed for each grid box. The zonal means calculated are generally within
 1617 2 K/100 sfu of other reported solar response coefficients, but there is a strong latitudinal
 1618 and seasonal dependence (strongest solar flux response in mid-latitude winter hemisphere
 1619 – near zero response in high latitude summer), iii) we have assumed no lag between solar

1620 flux variations and the temperature response, whereas previous work for the Davis response
1621 for example indicates a ~160 day lag is optimal [at least for Davis](#) (French and Klekociuk,
1622 2011) and iv) for comparison with other hydroxyl temperature long-term trends we assume
1623 the global OH layer height is well matched with the Aura/MLS 0.00464 hPa level.

1624 To address uncertainties about the solar response coefficient ([item ii above](#)) we
1625 have recalculated the global trends assuming a fixed response for each grid box (4.2 K/100
1626 sfu [as](#) derived from the Davis observations) and also as zonal means but for a lag of 160
1627 days (F10.7 leads T) as previously found for Davis. ~~These plots analysis are available in~~
1628 ~~the supplementary material and determines show~~ that, by and large, the warming and
1629 cooling patterns observed in Figure 6 do not change significantly for the different solar
1630 cycle [response components computations](#).

1631 While the WACCM-X results presented by Qian et al. (2019) are in reasonable
1632 agreement with the OH temperature behaviour measured at Davis Station, the zonally
1633 averaged pattern of solar cycle response and linear trend obtained from WACCM-X differs
1634 considerably from that obtained from ~~an~~ analysis of the Aura/MLS data at the 0.00464 hPa
1635 level shown in Figure 6. In the Aura/MLS results, the solar response in both hemispheres
1636 in winter show a great deal more variation as a function of latitude than is evident in the
1637 WACCM-X results at 87 km (Figure 4 of Qian et al., 2019). The zonally averaged
1638 Aura/MLS pattern shows maxima (~~~6 K/100sfu~~) in southern mid-latitudes in the ~~Southern~~
1639 ~~Hemisphere (SH)~~SH winter, ~~and similarly while the~~ maximum (~~although a smaller peak~~
1640 ~~~4 K/100sfu compared to the SH response~~) ~~is~~ in northern mid-latitudes in the ~~NH~~~~Northern~~
1641 ~~Hemisphere (NH)~~ winter. The solar cycle response is essentially zero at 82° north and
1642 south during the NH winter months, but it is of the order of 3 K/~~100sfu decade~~ at 82° south
1643 in SH winter. The ~~southern hemisphere~~SH winter months have the largest variation with
1644 a pronounced maximum in the latitude range ~10° S to 40° S. (The maximum also shows

1645 longitudinal structure with a much broader maximum between 90° east and 90° west which
1646 is centred at higher southern latitudes.) Several authors (Perminov et al., 2014; Pertsev and
1647 Perminov, 2008) have reported that winter OH* temperatures are more sensitive to the
1648 solar flux variation than summer temperatures and t. This agrees with the Aura/MLS
1649 variation shown herein Figure 6.

1650 The ~~WACCM-X~~ long term trend modelled by WACCM-X is predominantly
1651 negative or zero at the altitude of the OH layer (87 km) at all latitudes and in all months
1652 apart from February, November and December, when a positive trend of up to ~3 K/decade
1653 is present at high southern latitudes (see Fig 3. in Qian et al., 2019). Aura/MLS results also
1654 show a predominantly slight negative trend ~0.5-1 K/decade, except at the equator, and at
1655 mid-latitudes in the SH winter months.

1656 Solomon et al. (2018) simulated the anthropogenic global change through the entire
1657 atmosphere using WACCM-X in a free-running mode (i.e., lower atmosphere below 50
1658 km not constrained by ECMWF reanalysis data) using constant low solar activity
1659 conditions. They find substantial cooling in the mesosphere of the order of -1 K/decade,
1660 increasing to -2.8K/decade in the thermosphere. Temperature decreases were small near
1661 the mesopause compared with the variation in the annual mean thus making trends there
1662 somewhat uncertain. Solomon et al. (2018) conclude that inconsistent observational results
1663 in the mesopause region, together with little or no global mean trends is due to the
1664 dominance of dynamical processes in controlling mesopause temperature, which exhibits
1665 significant inter-annual variability, even without variable solar forcing.

1666 The SABER dataset (2002-2015) was used by Tang et al. (2016) to study the
1667 response of the cold-point temperature of the mesopause (T-CPM) to solar activity. The
1668 results showed that the T-CPM is significantly correlated to solar activity at all latitudes,
1669 and the solar response becomes stronger with increasing latitude. The solar-cycle

1670 dependence of the mesopause cold point temperature (T-CPM) is due to the relative
1671 importance of CO₂ and NO infrared cooling (Tang et al., 2016). NO density at solar max
1672 is about three times that at solar minimum. Consequently, CO₂ cooling is relatively less
1673 important at solar maximum, but is the dominant cooling mechanism during solar
1674 minimum.

1675 Values of the solar response of T-CPM reported by Tang et al. (2016) increased
1676 from 2.82 ± 0.73 K/100 sfu at 0-10° S to 6.35 ± 1.16 K/100 sfu at 60-70° S (see their Fig
1677 5(a)). Correlation coefficients of mesopause temperature with F10.7 cm solar irradiance
1678 data were higher for mid-latitudes (> 0.9) than at the equator (~0.7) and at higher latitude
1679 (see their Fig 5(b)). The ~~value correlation coefficient~~ found for 70° S (~0.8) is consistent
1680 with the ~~correlation coefficient value~~ obtained for the OH* temperatures (Figure 13(a) (*R*²
1681 = 0.584) ~~or R = 0.76~~) obtained in ~~this~~ ~~this~~ work. At low latitudes, one would expect
1682 the QBO and ENSO to be significant factors ~~there~~ (see e.g., Nath and Sridharan, 2014), but
1683 at high latitudes, gravity wave activity is a candidate for the missing variance. Inter-annual
1684 variations of GWs at high latitudes are correlated with the strength of the polar vortex. A
1685 stronger polar vortex filters out more eastward propagating GWs, thus leading to more
1686 westward GW drag, which drives stronger meridional circulation (Karlsson and Shepherd,
1687 2018).

1688 Although the altitude of the [mesospheric](#) cold point changes with season (e.g., Yuan
1689 et al., 2019) ~~and~~ tends to be higher than the centroid [height](#) of the OH* layer, ~~t~~ the global
1690 solar response value obtained for T-CPM (4.89 ± 0.67 K/100 SFU) is in good agreement
1691 with the solar response coefficient derived from ground-based OH* observations.

1692 The solar response of the T-CPM in Tang et al. (2016) shows some significant
1693 differences from the results in Figure 6 (zonal mean cycle from Aura/MLS) of this work.
1694 The solar response of the T-CPM increases more or less monotonically with latitude,

Formatted: Font: Italic

Formatted: Superscript

Formatted: Font: Italic

1695 whereas the solar response ~~registered~~ observed by Aura/MLS maximises at higher mid-
1696 latitudes. Of course the height of the T-CPM is some 7 km higher on average as indicated
1697 in Figure 9 (b) of Tang et al. (2016).

1698 ~~Several authors (Perminov et al., 2014; Pertsev and Perminov, 2008) have reported that~~
1699 ~~winter OH* temperatures are more sensitive to the solar flux variation than summer~~
1700 ~~temperatures. This agrees with the Aura/MLS variation shown in Figure 6.~~

Formatted: Font: Times New Roman, 12 pt

Formatted: Font: Times New Roman, 12 pt

1701 As a final comment on the global trends, it is noted that the largest errors in the
1702 linear trend fit for the SH winter understandably occur coincident with the regions
1703 positively or negatively correlated with the QOO (not shown here). The fit can be
1704 significantly improved if the QOO component can be understood and modelled. We
1705 investigate the QOO in detail in part 2 of this work.

Formatted: Plain Text

1706 ~~(cf. figure 3. i.e., eastern Antarctic polar cap, southern Pacific and southern Indian~~
1707 ~~oceans). This is understandable if there is a significant QOO signal superposed on the~~
1708 ~~underlying long term linear trend.~~

1710 6. Summary and Conclusions

1711 We provide updates for the long-term trend and solar cycle response derived from
1712 24 years of spectrometer observations of hydroxyl airglow at Davis Research Station,
1713 Antarctica (68° S, 78° E). A cooling trend in the mean winter temperatures [D106-259] of
1714 -1.20 ± 0.51 K/decade (95% confidence limits -0.14 K/decade $< L < -2.26$ K/decade) is
1715 obtained coupled with a solar cycle response coefficient of 4.30 ± 1.02 K/100sfu (95%
1716 confidence limits 2.2 K/100sfu $< S < 6.4$ K/100sfu). The observed cooling is consistent
1717 with radiative cooling due to increasing CO₂ concentrations and a rate of -0.06 K/ppmCO₂
1718 or -0.22 K/%CO₂ is implied (ignoring possible contributions of stratospheric ozone change

1719 to the trend). A significant note is that a new record low winter-mean temperature was set
1720 for the Davis measurements in 2018, with a value of 198.3 K, which is 1.7 K below the
1721 previous minimum recorded in 2009 (200.0 K). An examination of the seasonal variation
1722 in the trend fit parameters reveals very little (no significant) long-term trend occurs over
1723 the ~~2-two~~ midwinter months of June and July, but 95% significant trends of -1.5 to -2.6
1724 K/decade during the April-May and August-October intervals. From examination of
1725 TIMED/SABER VER profiles we see no evidence that the trend results obtained can be
1726 significantly attributed to a change in the height of the OH layer.

1727 We do not see evidence of a trend break or a change in the nature of the underlying
1728 trend after accounting for the solar cycle response in the Davis OH temperatures, however,
1729 this simple solar-cycle and linear trend model fit accounts for only 58% of the temperature
1730 variability. The remaining variability reveals evidence of a temperature oscillation on a
1731 quasi-quadrennial (~4 year period) timescale.

1732 We compare our observations with Aura/MLS version v4.2 level 2 data over the
1733 last 14 years when these satellite data are available and find close agreement (a best fit [to](#)
1734 [the variance in mean winter anomaly](#)) with the 0.00464 hPa (native Aura/MLS retrieval)
1735 pressure level values. The solar cycle response, long-term trend and underlying QOO
1736 residuals are consistent with the Davis observations. Consequently, we derive global maps
1737 of Aura/MLS trend and solar response coefficients for the SH and NH winter periods to
1738 compare with other observers and models. Significant patterns for the zonally averaged
1739 solar cycle response are maxima in southern mid-latitudes in the [Southern Hemisphere](#)
1740 ~~(SH)~~SH winter and in northern mid-latitudes in the [Northern Hemisphere \(NH\)](#)NH winter.
1741 Long term trends are ~~a~~-predominantly slight negative (~0.5-1 K/decade), except at the
1742 equator, and at mid-latitudes in the SH winter months. Comparisons are also made with the
1743 WACCM-X model and mesopause cold point temperature versus solar activity study using

1744 TIMED/SABER data of Tang et al. (2016), both of which reveal significant differences in
1745 the zonally averaged patterns of solar cycle response and linear trend compared to the
1746 Aura/MLS data at 0.00464 hPa.

1747 Further analysis using the datasets described here ~~are is~~ undertaken to ~~examine~~
1748 ~~explore~~ the ~~residual~~-QQO signal ~~that this analysis has revealed~~revealed in the residual
1749 temperatures. A second part of this paper “Analysis of 24 years of mesopause region OH
1750 rotational temperature observations at Davis, Antarctica. Part 2: Evidence of a quasi-
1751 quadrennial oscillation (QQO) in the polar mesosphere.” concerns this observation.

1752

1753 Data Availability

1754 All Davis hydroxyl rotational data described in this manuscript are available through the
1755 Australian Antarctic Data Centre website (ref project AAS4157) via the following link
1756 https://data.aad.gov.au/metadata/records/Davis_OH_airglow . The satellite data used in
1757 this paper were obtained from the Aura/MLS data centre (see <https://mls.jpl.nasa.gov>), the
1758 SABER data centre (see <http://saber.gats-inc.com/data.php>) and are publicly available.

1759

1760 Author Contribution

1761 WJRF managed data collection, performed data analysis, prepared manuscript with
1762 contributions from all co-authors

1763 FJM analysis of SABER data, manuscript editing, figures, references

1764 ARK analysis of Aura/MLS satellite data, manuscript editing.

1765

1766 **Competing Interests**

1767 The authors declare that they have no conflict of interest.

1768

1769 **Acknowledgements**

1770 The authors thank the dedicated work of the Davis optical physicists and
1771 engineers over many years in the collection of airglow data and calibration of
1772 instruments. This work is supported by the Australian Antarctic Science Advisory
1773 Council (project AAS 4157).

1774 The satellite data used in this paper were obtained from the Aura/MLS data centre
1775 (see <https://mls.jpl.nasa.gov>), the SABER data centre (see [http://saber.gats-](http://saber.gats-inc.com/data.php)
1776 [inc.com/data.php](http://saber.gats-inc.com/data.php)) and are publicly available. We thank those teams and acknowledge the
1777 use of these data sets.

1778 This work contributes to the understanding of mesospheric change processes
1779 coordinated through the Network for Detection of Mesospheric Change (see
1780 <https://ndmc.dlr.de/>)

1781 **References**

1782 Akmaev, R. A., Fomichev, V. I. and Zhu, X.: Impact of middle-atmospheric composition
1783 changes on greenhouse cooling in the upper atmosphere, *J. Atmos. Solar-Terrestrial*
1784 *Phys.*, 68(17), 1879–1889, doi:10.1016/j.jastp.2006.03.008, 2006.

1785 Ammosov, P., Gavrielyeva, G., Ammosova, A. and Koltovskoi, I.: Response of the
1786 mesopause temperatures to solar activity over Yakutia in 1999–2013, *Adv. Sp. Res.*,
1787 54(12), 2518–2524, doi:10.1016/J.ASR.2014.06.007, 2014.

1788 Azeem, S. M. I., Sivjee, G. G., Won, Y.-I. and Mutiso, C.: Solar cycle signature and

1789 secular long-term trend in OH airglow temperature observations at South Pole,
1790 Antarctica, *J. Geophys. Res. Sp. Phys.*, 112(A1), n/a-n/a, doi:10.1029/2005JA011475,
1791 2007.

1792 Beig, G.: Trends in the mesopause region temperature and our present understanding-an
1793 update, *Phys. Chem. Earth*, 31(1–3), 3–9, doi:10.1016/j.pce.2005.03.007, 2006.

1794 Beig, G.: Long-term trends in the temperature of the mesosphere/lower thermosphere
1795 region: 1. Anthropogenic influences, *J. Geophys. Res. Sp. Phys.*, 116(A2), n/a-n/a,
1796 doi:10.1029/2011JA016646, 2011a.

1797 Beig, G.: Long-term trends in the temperature of the mesosphere/lower thermosphere
1798 region: 2. Solar response, *J. Geophys. Res. Sp. Phys.*, 116(A2), n/a-n/a,
1799 doi:10.1029/2011JA016766, 2011b.

1800 Beig, G., Keckhut, P., Lowe, R. P., Roble, R. G., Mlynczak, M. G., Scheer, J., Fomichev,
1801 V. I., Offermann, D., French, W. J. R., Shepherd, M. G., Semenov, A. I., Remsberg, E.
1802 E., She, C. Y., Lübken, F. J., Bremer, J., Clemesha, B. R., Stegman, J., Sigernes, F. and
1803 Fadnavis, S.: Review of mesospheric temperature trends, *Rev. Geophys.*, 41(4),
1804 doi:10.1029/2002RG000121, 2003.

1805 Beig, G., Scheer, J., Mlynczak, M. G. and Keckhut, P.: Overview of the temperature
1806 response in the mesosphere and lower thermosphere to solar activity, *Rev. Geophys.*,
1807 46(3), doi:10.1029/2007RG000236, 2008.

1808 Bengtsson, L., Hagemann, S. and Hodges, K. I.: Can climate trends be calculated from
1809 reanalysis data?, *J. Geophys. Res.*, 109(D11), D11111, doi:10.1029/2004JD004536,
1810 2004.

1811 Bremer, J. and Peters, D.: Influence of stratospheric ozone changes on long-term trends in
1812 the meso- and lower thermosphere, *J. Atmos. Sol. Terr. Phys.*, 70, 1473–1481, 2008.

1813 Brooke, J. S. A., Bernath, P. F., Western, C. M., Sneden, C., Afşar, M., Li, G. and

1814 Gordon, I. E.: Line strengths of rovibrational and rotational transitions in the X 2 Π
1815 ground state of OH, *J. Quant. Spectrosc. Radiat. Transf.*, 168, 142–157,
1816 doi:10.1016/j.jqsrt.2015.07.021, 2016.

1817 Burns, G. B., Kawahara, T. D., French, W. J. R., Nomura, A. and Klekociuk, A. R.: A
1818 comparison of hydroxyl rotational temperatures from Davis (69°S, 78°E) with sodium
1819 lidar temperatures from Syowa (69°S, 39°E), *Geophys. Res. Lett.*, 30(1),
1820 doi:10.1029/2002GL016413, 2003.

1821 Clemesha, B., Takahashi, H., Simonich, D., Gobbi, D. and Batista, P.: Experimental
1822 evidence for solar cycle and long-term change in the low-latitude MLT region, *J. Atmos.*
1823 *Solar-Terrestrial Phys.*, 67(1–2), 191–196, doi:10.1016/j.jastp.2004.07.027, 2005.

1824 Espy, P. J., Ochoa Fernández, S., Forkman, P., Murtagh, D. and Stegman, J.: The role of
1825 the QBO in the inter-hemispheric coupling of summer mesospheric temperatures, *Atmos.*
1826 *Chem. Phys.*, 11(2), 495–502, doi:10.5194/acp-11-495-2011, 2011.

1827 Fomichev, V. I., Jonsson, A. I., de Grandpré, J., Beagley, S. R., McLandress, C.,
1828 Semeniuk, K. and Shepherd, T. G.: Response of the middle atmosphere to CO2 doubling:
1829 Results from the Canadian middle atmosphere model, *J. Clim.*, 20(7), 1121–1144,
1830 doi:10.1175/JCLI4030.1, 2007.

1831 French, W. J. R., Klekociuk, A. R., Mulligan, F. J.: Analysis of 24 years of mesopause
1832 region OH rotational temperature observations at Davis, Antarctica. Part 2: Evidence of a
1833 quasi-quadrennial oscillation (QO) in the polar mesosphere., *Atmos. Chem. Phys.*,
1834 [2019](#)~~2020~~.

1835 French, W. J. R. and Burns, G. B.: The influence of large-scale oscillations on long-term
1836 trend assessment in hydroxyl temperatures over Davis, Antarctica, *J. Atmos. Solar-*
1837 *Terrestrial Phys.*, 66(6–9), 493–506, doi:10.1016/j.jastp.2004.01.027, 2004.

1838 French, W. J. R. and Klekociuk, A. R.: Long-term trends in Antarctic winter hydroxyl

1839 temperatures, *J. Geophys. Res.*, 116(D4), D00P09, doi:10.1029/2011JD015731, 2011.

1840 French, W. J. R. and Mulligan, F. J.: Stability of temperatures from TIMED/SABER
1841 v1.07 (2002–2009) and Aura/MLS v2.2 (2004–2009) compared with OH(6-2)
1842 temperatures observed at Davis Station, Antarctica, *Atmos. Chem. Phys.*, 10(23), 11439–
1843 11446, doi:10.5194/acp-10-11439-2010, 2010.

1844 French, W. J. R., Burns, G. B., Finlayson, K., Greet, P. A., Lowe, R. P. and Williams, P.
1845 F. B.: Hydroxyl (6–2) airglow emission intensity ratios for rotational temperature
1846 determination, *Ann. Geophys.*, 18(10), 1293–1303, doi:10.1007/s00585-000-1293-2,
1847 2000.

1848 Gao, H., Xu, J. and Chen, G.: The responses of the nightglow emissions observed by the
1849 TIMED/SABER satellite to solar radiation, *J. Geophys. Res. Sp. Phys.*, 121(2), 1627–
1850 1642, doi:10.1002/2015JA021624, 2016.

1851 García-Comas, M., López-González, M. J., González-Galindo, F., de la Rosa, J. L.,
1852 López-Puertas, M., Shepherd, M. G. and Shepherd, G. G.: Mesospheric OH layer altitude
1853 at midlatitudes: variability over the Sierra Nevada Observatory in Granada, Spain (37° N,
1854 3° W), *Ann. Geophys.*, 35(5), 1151–1164, doi:10.5194/angeo-35-1151-2017, 2017.

1855 Garcia, R. R., López-Puertas, M., Funke, B., Marsh, D. R., Kinnison, D. E., Smith, A. K.
1856 and González-Galindo, F.: On the distribution of CO₂ and CO in the mesosphere and
1857 lower thermosphere, *J. Geophys. Res.*, 119(9), 5700–5718, doi:10.1002/2013JD021208,
1858 2014.

1859 Garcia, R. R., Yue, J. and Russell, J. M.: Middle atmosphere temperature trends in the 20
1860 th and 21 st centuries simulated with the Whole Atmosphere Community Climate Model
1861 (WACCM) , *J. Geophys. Res. Sp. Phys.*, doi:10.1029/2019ja026909, 2019.

1862 Greet, P. A., French, W. J. R., Burns, G. B., Williams, P. F. B., Lowe, R. P. and
1863 Finlayson, K.: OH(6-2) spectra and rotational temperature measurements at Davis,

1864 Antarctica, *Ann. Geophys.*, 16(1), 77–89, doi:10.1007/s00585-997-0077-3, 1997.

1865 Grygalashvyly, M., Sonnemann, G. R., Lübken, F. J., Hartogh, P. and Berger, U.:

1866 Hydroxyl layer: Mean state and trends at midlatitudes, *J. Geophys. Res. Atmos.*, 119(21),
1867 12,391–12,419, doi:10.1002/2014JD022094, 2014.

1868 Holmen, S. E., Dyrlund, M. E. and Sigernes, F.: Mesospheric temperatures derived from
1869 three decades of hydroxyl airglow measurements from Longyearbyen, Svalbard (78°N),
1870 *Acta Geophys.*, 62(2), 302–315, doi:10.2478/s11600-013-0159-4, 2014.

1871 Huang, T.-Y.: Influences of CO₂ increase, solar cycle variation, and geomagnetic activity
1872 on airglow from 1960 to 2015, *J. Atmos. Solar-Terrestrial Phys.*, 171, 164–175,
1873 doi:10.1016/J.JASTP.2017.06.008, 2018.

1874 Jacobi, C., Lilienthal, F., Geißler, C. and Krug, A.: Long-term variability of mid-latitude
1875 mesosphere-lower thermosphere winds over Collm (51°N, 13°E), *J. Atmos. Solar-*
1876 *Terrestrial Phys.*, 136, 174–186, doi:10.1016/j.jastp.2015.05.006, 2015.

1877 Kalicinsky, C., Knieling, P., Koppmann, R., Offermann, D., Steinbrecht, W. and Wintel,
1878 J.: Long-term dynamics of OH * temperatures over central Europe: trends and solar
1879 correlations, *Atmos. Chem. Phys.*, 16(23), 15033–15047, doi:10.5194/acp-16-15033-
1880 2016, 2016.

1881 Kalicinsky, C., Peters, D. H. W., Entzian, G., Knieling, P. and Matthias, V.:

1882 Observational evidence for a quasi-bidecadal oscillation in the summer mesopause region
1883 over Western Europe, *J. Atmos. Solar-Terrestrial Phys.*, 178, 7–16,
1884 doi:10.1016/j.jastp.2018.05.008, 2018.

1885 Karlsson, B. and Shepherd, T. G.: The improbable clouds at the edge of the atmosphere,
1886 *Phys. Today*, 71(6), 30–36, doi:10.1063/PT.3.3946, 2018.

1887 Kim, G., Kim, J.-H., Kim, Y. H. and Lee, Y. S.: Long-term trend of mesospheric
1888 temperatures over Kiruna (68°N, 21°E) during 2003–2014, *J. Atmos. Solar-Terrestrial*

1889 Phys., 161, 83–87, doi:10.1016/j.jastp.2017.06.018, 2017.

1890 Kvifte, G. and G.: Temperature measurements from OH bands, *Planet. Space Sci.*, 5(2),
1891 153–157, doi:10.1016/0032-0633(61)90090-3, 1961.

1892 Langhoff, S. R., Werner, H. J. and Rosmus, P.: Theoretical Transition Probabilities for
1893 the OH Meinel System, *J. Mol. Spectrosc.*, 118, 507–529, 1986.

1894 Laštovička, J. and Jan: A review of recent progress in trends in the upper atmosphere, *J.*
1895 *Atmos. Solar-Terrestrial Phys.*, 163, 2–13, doi:10.1016/j.jastp.2017.03.009, 2017.

1896 Liu, G. and Shepherd, G. G.: An empirical model for the altitude of the OH nightglow
1897 emission, *Geophys. Res. Lett.*, 33(9), L09805, doi:10.1029/2005GL025297, 2006.

1898 Livesey, Nathaniel J., William G. Read, Paul A. Wagner, Lucien Froidevaux, A. L.,
1899 Gloria L. Manney, Luis F. Millán Valle, Hugh C. Pumphrey, M. L. S., Michael J.
1900 Schwartz, Shuhui Wang, Ryan A. Fuller, Robert F. Jarnot, B. W. K. and Elmain
1901 Martinez, R. R. L.: Earth Observing System (EOS) Aura Microwave Limb Sounder
1902 (MLS) Version 4.2x Level 2 data quality and description document Version 4.2x–3.1, , 1–
1903 163 [online] Available from: [https://mls.jpl.nasa.gov/data/v4-](https://mls.jpl.nasa.gov/data/v4-2_data_quality_document.pdf)
1904 [2_data_quality_document.pdf](https://mls.jpl.nasa.gov/data/v4-2_data_quality_document.pdf), 2018.

1905 van der Loo, M. P. J. and Groenenboom, G. C.: Theoretical transition probabilities for the
1906 OH Meinel system, *J. Chem. Phys.*, 126(11), 114314, doi:10.1063/1.2646859, 2007.

1907 López-Puertas, M., Funke, B., Jurado-Navarro, A., García-Comas, M., Gardini, A.,
1908 Boone, C. D., Rezac, L. and Garcia, R. R.: Validation of the MIPAS CO₂ volume mixing
1909 ratio in the mesosphere and lower thermosphere and comparison with WACCM
1910 simulations, *J. Geophys. Res.*, 122(15), 8345–8366, doi:10.1002/2017JD026805, 2017.

1911 Lübken, F.-J., Berger, U. and Baumgarten, G.: Temperature trends in the midlatitude
1912 summer mesosphere, *J. Geophys. Res. Atmos.*, 118(24), 13,347-13,360,
1913 doi:10.1002/2013JD020576, 2013.

1914 Mertens, C. J., Mlynczak, M. G., López-Puertas, M., Wintersteiner, P. P., Picard, R. H.,
1915 Winick, J. R., Gordley, L. L. and Russell III, J. M.: Retrieval of kinetic temperature and
1916 carbon dioxide abundance from nonlocal thermodynamic equilibrium limb emission
1917 measurements made by the SABER experiment on the TIMED satellite, in Proc SPIE
1918 4882, Remote Sensing of Clouds and the Atmosphere VII, pp. 162–171., 2003.
1919 Mies, F. H.: Calculated vibrational transition probabilities of OH(X2Π), J. Mol.
1920 Spectrosc., 53(2), 150–188, doi:10.1016/0022-2852(74)90125-8, 1974.
1921 Mulligan, F. J., Dyrland, M. E., Sigernes, F. and Deehr, C. S.: Inferring hydroxyl layer
1922 peak heights from ground-based measurements of OH(6-2) band integrated emission rate
1923 at Longyearbyen (78° N, 16° E), Ann. Geophys., 27(11), 4197–4205,
1924 doi:10.5194/angeo-27-4197-2009, 2009.
1925 Murphy, D. J., French, W. J. R. and Vincent, R. A.: Long-period planetary waves in the
1926 mesosphere and lower thermosphere above Davis, Antarctica, J. Atmos. Solar-Terrestrial
1927 Phys., 69(17–18), 2118–2138, doi:10.1016/J.JASTP.2007.06.008, 2007.
1928 Nath, O. and Sridharan, S.: Long-term variabilities and tendencies in zonal mean
1929 TIMED–SABER ozone and temperature in the middle atmosphere at 10–15°N, J. Atmos.
1930 Solar-Terrestrial Phys., 120, 1–8, doi:10.1016/j.jastp.2014.08.010, 2014.
1931 Noll S., Winkler, H., Goussev, O. and Proxauf, O.: OH level populations and accuracies
1932 of Einstein-A coefficients from hundreds of measured lines, Atmospheric Chem. Phys.
1933 [online] Available from: <https://doi.org/10.5194/acp-2019-1102>, 2020.
1934 Offermann, D., Jarisch, M., Donner, M., Steinbrecht, W. and Semenov, A. I.: OH
1935 temperature re-analysis forced by recent variance increases, J. Atmos. Solar-Terrestrial
1936 Phys., 68(17), 1924–1933, doi:10.1016/J.JASTP.2006.03.007, 2006.
1937 Offermann, D., Hoffmann, P., Knieling, P., Koppmann, R., Oberheide, J. and Steinbrecht,
1938 W.: Long-term trends and solar cycle variations of mesospheric temperature and

1939 dynamics, *J. Geophys. Res.*, 115(D18), D18127, doi:10.1029/2009JD013363, 2010.

1940 Perminov, V. I., Semenov, A. I., Medvedeva, I. V. and Pertsev, N. N.: Temperature
1941 variations in the mesopause region according to the hydroxyl-emission observations at
1942 midlatitudes, *Geomagn. Aeron.*, 54(2), 230–239, doi:10.1134/S0016793214020157,
1943 2014.

1944 Perminov, V. I., Semenov, A. I., Pertsev, N. N., Medvedeva, I. V., Dalin, P. A. and
1945 Sukhodoev, V. A.: Multi-year behaviour of the midnight OH* temperature according to
1946 observations at Zvenigorod over 2000–2016, *Adv. Sp. Res.*, 61(7), 1901–1908,
1947 doi:10.1016/J.ASR.2017.07.020, 2018.

1948 Pertsev, N. and Perminov, V.: Response of the mesopause airglow to solar activity
1949 inferred from measurements at Zvenigorod, Russia, *Ann. Geophys.*, 26(5), 1049–1056,
1950 doi:10.5194/angeo-26-1049-2008, 2008.

1951 Picone, J. M., Hedin, A. E., Drob, D. P. and Aikin, A. C.: NRLMSISE-00 empirical
1952 model of the atmosphere: Statistical comparisons and scientific issues, *J. Geophys. Res.*
1953 *Sp. Phys.*, doi:10.1029/2002JA009430, 2002.

1954 Qian, L., Jacobi, C. and McInerney, J.: Trends and Solar Irradiance Effects in the
1955 Mesosphere, *J. Geophys. Res. Sp. Phys.*, 124(2), 1343–1360,
1956 doi:10.1029/2018JA026367, 2019.

1957 Reid, I. M., Spargo, A. J., Woithe, J. M., Klekociuk, A. R., Younger, J. P. and Sivjee, G.
1958 G.: Seasonal MLT-region nightglow intensities, temperatures, and emission heights at a
1959 Southern Hemisphere midlatitude site, *Ann. Geophys.*, 35(3), 567–582,
1960 doi:10.5194/angeo-35-567-2017, 2017.

1961 Reisin, E. R., Scheer, J., Dyrland, M. E., Sigernes, F., Deehr, C. S., Schmidt, C.,
1962 Höppner, K., Bittner, M., Ammosov, P. P., Gavril'yeva, G. A., Stegman, J., Perminov, V.
1963 I., Semenov, A. I., Knieling, P., Koppmann, R., Shiokawa, K., Lowe, R. P., López-

1964 González, M. J., Rodríguez, E., Zhao, Y., Taylor, M. J., Buriti, R. A., Espy, P. J., French,
1965 W. J. R., Eichmann, K.-U., Burrows, J. P. and von Savigny, C.: Traveling planetary wave
1966 activity from mesopause region airglow temperatures determined by the Network for the
1967 Detection of Mesospheric Change (NDMC), *J. Atmos. Solar-Terrestrial Phys.*, 119, 71–
1968 82, doi:10.1016/J.JASTP.2014.07.002, 2014.

1969 Rezac, L., Jian, Y., Yue, J., Russell, J. M., Kutepov, A., Garcia, R., Walker, K. and
1970 Bernath, P.: Validation of the global distribution of CO₂ volume mixing ratio in the
1971 mesosphere and lower thermosphere from SABER, *J. Geophys. Res.*, 120(23), 12,067–
1972 12,081, doi:10.1002/2015JD023955, 2015.

1973 Roble, R. G.: On the feasibility of developing a global atmospheric model extending from
1974 the ground to the exosphere, pp. 53–67., 2000.

1975 Roble, R. G. and Dickinson, R. E.: How will changes in carbon dioxide and methane
1976 modify the mean structure of the mesosphere and thermosphere?, *Geophys. Res. Lett.*,
1977 16(12), 1441–1444, doi:10.1029/GL016i012p01441, 1989.

1978 von Savigny, C.: Variability of OH(3–1) emission altitude from 2003 to 2011: Long-term
1979 stability and universality of the emission rate–altitude relationship, *J. Atmos. Solar-*
1980 *Terrestrial Phys.*, 127, 120–128, doi:10.1016/J.JASTP.2015.02.001, 2015.

1981 von Savigny, C., McDade, I. C., Eichmann, K. U. and Burrows, J. P.: On the dependence
1982 of the OH* Meinel emission altitude on vibrational level: SCIAMACHY observations
1983 and model simulations, *Atmospheric Chem. Phys.*, 12, 8813–8828, doi:10.5194/acp-12-
1984 8813-2012, 2012.

1985 Scheer, J., Reisin, E. R. and Mandrini, C. H.: Solar activity signatures in mesopause
1986 region temperatures and atomic oxygen related airglow brightness at El Leoncito,
1987 Argentina, *J. Atmos. Solar-Terrestrial Phys.*, 67(1–2), 145–154,
1988 doi:10.1016/j.jastp.2004.07.023, 2005.

1989 Schmidt, H., Brasseur, G. P., Charron, M., Manzini, E., Giorgetta, M. A., Diehl, T.,

1990 Fomichev, V. I., Kinnison, D., Marsh, D. and Walters, S.: The HAMMONIA chemistry

1991 climate model: Sensitivity of the mesopause region to the 11-year solar cycle and CO₂

1992 doubling, *J. Clim.*, 19(16), 3903–3931, doi:10.1175/JCLI3829.1, 2006.

1993 Schwartz, M. J., Lambert, A., Manney, G. L., Read, W. G., Livesey, N. J., Froidevaux,

1994 L., Ao, C. O., Bernath, P. F., Boone, C. D., Cofield, R. E., Daffer, W. H., Drouin, B. J.,

1995 Fetzer, E. J., Fuller, R. A., Jarnot, R. F., Jiang, J. H., Jiang, Y. B., Knosp, B. W., Krüger,

1996 K., Li, J.-L. F., Mlynczak, M. G., Pawson, S., Russell, J. M., Santee, M. L., Snyder, W.

1997 V., Stek, P. C., Thurstans, R. P., Tompkins, A. M., Wagner, P. A., Walker, K. A., Waters,

1998 J. W. and Wu, D. L.: Validation of the Aura Microwave Limb Sounder temperature and

1999 geopotential height measurements, *J. Geophys. Res.*, 113(D15),

2000 doi:10.1029/2007jd008783, 2008.

2001 Sivakandan, M., Ramkumar, T. K., Taori, A., Rao, V. and Niranjana, K.: Long-term

2002 variation of OH peak emission altitude and volume emission rate over Indian low

2003 latitudes, *J. Atmos. Solar-Terrestrial Phys.*, 138–139, 161–168,

2004 doi:10.1016/j.jastp.2016.01.012, 2016.

2005 Sivjee, G. G.: Airglow hydroxyl emissions, *Planet. Space Sci.*, 40(2–3), 235–242,

2006 doi:10.1016/0032-0633(92)90061-R, 1992.

2007 Solomon, S. C., Liu, H., Marsh, D. R., McInerney, J. M., Qian, L. and Vitt, F. M.: Whole

2008 Atmosphere Simulation of Anthropogenic Climate Change, *Geophys. Res. Lett.*, 45(3),

2009 1567–1576, doi:10.1002/2017GL076950, 2018.

2010 Sonnemann, G. R., Hartogh, P., Berger, U. and Grygalskaya, M.: Hydroxyl layer: trend

2011 of number density and intra-annual variability, *Ann. Geophys.*, 33(6), 749–767,

2012 doi:10.5194/angeo-33-749-2015, 2015.

2013 Tang, C., Liu, D., Wei, H., Wang, Y., Dai, C., Wu, P., Zhu, W. and Rao, R.: The

2014 response of the temperature of cold-point mesopause to solar activity based on SABER
2015 data set, *J. Geophys. Res. Sp. Phys.*, 121(7), 7245–7255, doi:10.1002/2016JA022538,
2016 2016.

2017 Teiser, G. and von Savigny, C.: Variability of OH(3-1) and OH(6-2) emission altitude
2018 and volume emission rate from 2003 to 2011, *J. Atmos. Solar-Terrestrial Phys.*, 161, 28–
2019 42, doi:10.1016/J.JASTP.2017.04.010, 2017.

2020 Thulasiraman, S. and Nee, J. B.: Further evidence of a two-level mesopause and its
2021 variations from UARS high-resolution Doppler imager temperature data, *J. Geophys.*
2022 *Res.*, 107(D18), 4355, doi:10.1029/2000JD000118, 2002.

2023 Turnbull, D. N. and Lowe, R. P.: New hydroxyl transition probabilities and their
2024 importance in airglow studies, *Planet. Space Sci.*, 37(6), 723–738, doi:10.1016/0032-
2025 0633(89)90042-1, 1989.

2026 Venturini, M. S., Bageston, J. V., Caetano, N. R., Peres, L. V., Bencherif, H. and Schuch,
2027 N. J.: Mesopause region temperature variability and its trend in southern Brazil, *Ann.*
2028 *Geophys.*, 36(2), 301–310, doi:10.5194/angeo-36-301-2018, 2018.

2029 Wüst, S., Bittner, M., Yee, J.-H., Mlynczak, M. G. and Russell III, J. M.: Variability of
2030 the Brunt–Väisälä frequency at the OH* layer height, *Atmos. Meas. Tech.*, 10(12), 4895–
2031 4903, doi:10.5194/amt-10-4895-2017, 2017.

2032 Xu, J., Liu, H.-L., Yuan, W., Smith, A. K., Roble, R. G., Mertens, C. J., Russell, J. M.
2033 and Mlynczak, M. G.: Mesopause structure from Thermosphere, Ionosphere,
2034 Mesosphere, Energetics, and Dynamics (TIMED)/Sounding of the Atmosphere Using
2035 Broadband Emission Radiometry (SABER) observations, *J. Geophys. Res.*, 112(D9),
2036 D09102, doi:10.1029/2006JD007711, 2007.

2037 [Xu, J., Gao, H., Smith, A.K. and Zhu, Y. :Using TIMED/SABER nightglow observations](#)
2038 [to investigate hydroxyl emission mechanisms in the mesopause region. *J. Geophys.Res.*,](#)

2039 [117, D02301, doi:10.1029/2011JD016342, 2012.](#)

2040

2041 Yuan, T., Solomon, S. C., She, C. -Y., Krueger, D. A. and Liu, H. -L.: The long-term
2042 trends of nocturnal mesopause temperature and altitude revealed by Na lidar observations
2043 between 1990 and 2018 at mid-latitude, *J. Geophys. Res. Atmos.*, 2018JD029828,
2044 doi:10.1029/2018JD029828, 2019.

2045 von Zahn, U., Höffner, J., Eska, V. and Alpers, M.: The mesopause altitude: Only two
2046 distinctive levels worldwide?, *Geophys. Res. Lett.*, 23(22), 3231–3234,
2047 doi:10.1029/96GL03041, 1996.

2048